The Evolution of Calcite-Bearing Kimberlites by Melt-Rock Reaction – Evidence from Polymineralic Inclusions within Clinopyroxene and Garnet Megacrysts from Lac de Gras Kimberlites, Canada

Y. Bussweiler*[a], R.S. Stone[a], D.G. Pearson[a], R.W. Luth[a], T. Stachel[a], B.A. Kjarsgaard[b], A. Menzies[c]

[a)] Department of Earth and Atmospheric Sciences, University of Alberta, 126 ESB, Edmonton, AB T6G 2E3, Canada

[b)] Geological Survey of Canada, 601 Booth Street, Ottawa, ON, Canada K1A 0E8

[c)] Department of Geological Sciences, Universidad Católica del Norte, Antofagasta, Chile

*Corresponding author at: Department of Earth and Atmospheric Sciences, University of Alberta, 126 ESB, Edmonton, AB T6G 2E3, Canada. Tel.: +1 780 492 3265; fax:+1 780 492 2030. E-mail address: bussweil@ualberta.ca (Y. Bussweiler)

Acknowledgements

This study forms part of Y.B.'s Ph.D. research funded through D.G.P's Canada Excellence Research Chair. Y.B. is grateful for a University of Alberta Doctoral Recruitment Scholarship. The staff at Diavik Diamond Mine, especially Yuri Kinakin and Gus Fomradas, are thanked for generously allowing access to drill core for sampling. Juanita Bellinger at Rio Tinto is thanked for providing additional concentrate samples. The authors wish to acknowledge the support of CISEM (Centro de Investigación y Servicios Mineralógicos), Universidad Católica del Norte, Antofagasta, Chile for providing QEMSCAN® analytical time. At the University of Alberta, Sarah Gleeson is thanked for access to the fluid inclusion microscopy stage, Andrew Locock for assistance with EPMA, Yan Luo for assistance with LA-ICP-MS, and Chiranjeeb Sarkar for assistance with Sr column chemistry and TIMS.

We are grateful to Vadim Kamenetsky for his constructive and insightful review and for kindly allowing us to use Fig. 2d. We also thank Dante Danil for a very helpful review and Tim Grove for the editorial handling.

Abstract

Megacrystic (> 1 cm) clinopyroxene (Cr-diopside) and garnet (Cr-pyrope) xenocrysts within kimberlites from Lac de Gras (Northwest Territories, Canada) contain fully crystallized melt inclusions. These "polymineralic inclusions" have previously been interpreted to form by necking down of melts at mantle depths. We present a detailed petrographical and geochemical investigation of polymineralic inclusions and their host crystals to better understand how they form and what they reveal about the evolution of kimberlite melt. Genetically, the megacrysts are mantle xenocrysts with peridotitic chemical signatures indicating an origin within the lithospheric mantle (for the Cr-diopsides studied here ~4.6 GPa, 1015°C). Textural evidence for disequilibrium between the host crystals and their polymineralic inclusions (spongy rims in Cr-diopside, kelyphite in Cr-pyrope) is consistent with measured Sr isotopic disequilibrium. The preservation of disequilibrium establishes a temporal link to kimberlite eruption. In Cr-diopsides, polymineralic inclusions contain phlogopite, olivine, chromite, serpentine, and calcite. Abundant fluid inclusion trails surround the inclusions. In Cr-pyropes, the inclusions additionally contain Al-spinel, clinopyroxene, and dolomite. The major and trace element compositions of the inclusion phases are generally consistent with the early stages of kimberlite differentiation trends. Extensive chemical exchange between the host phases and the inclusions is indicated by enrichment of the inclusions in major components of the host crystals, such as Cr_2O_3 and Al_2O_3. This chemical evidence, along with phase equilibria constraints, supports the proposal that the inclusions within Cr-diopside record the decarbonation reaction: dolomitic melt + diopside → forsterite + calcite + CO_2, yielding the observed inclusion mineralogy and producing associated (CO_2-rich) fluid inclusions. Our study of polymineralic inclusions in megacrysts provides clear mineralogical and chemical evidence for an origin of kimberlite

that involves the reaction of high pressure dolomitic melt with diopside-bearing mantle assemblages producing a lower pressure melt that crystallizes a calcite-dominated assemblage in the crust.

Keywords

Kimberlite; Cr-rich Megacrysts; Polymineralic Inclusions; Melt Inclusions; Decarbonation Reaction; Kimberlite Evolution

Introduction

Despite over 100 years of research on kimberlites, the nature and origin of their primary melt(s) and their magmatic evolution path to the observed low pressure mineral assemblages remain controversial and elusive issues. The entrainment of, and reaction with, xenoliths and xenocrysts spanning the entire lithosphere greatly complicates the search for the primary kimberlite melt, and the picture is further obscured by post-emplacement alteration (Mitchell 1986; Mitchell 1995; Price et al. 2000; Kopylova et al. 2007; Sparks et al. 2009; Kjarsgaard et al. 2009). Two of the key issues in kimberlite research that are still debated are: 1) Whether the primary kimberlite is carbonatitic (Dawson 1971; Dawson and Hawthorne 1973; Russell et al. 2012; Kamenetsky and Yaxley 2015; Kamenetsky 2016), a carbonated silicate melt (e.g., Nielsen and Sand 2008; Brey et al. 2008), or a highly saline carbonatite (e.g., Kamenetsky et al. 2012); and: 2) The mechanism for generating the calcite-bearing kimberlites observed in the crust – all experimental evidence suggests that a primary melt formed from the melting of a peridotitic source must produce Mg-rich carbonate, namely dolomite (e.g., Wyllie and Huang 1975; Dalton and Presnall 1998a).

The idea that kimberlites start off as end-member carbonatites that then react with mantle phases, mostly orthopyroxene (opx), to create a more Si- and Mg-rich melt has recently gained ground following experimental studies (Russell et al. 2012; Kamenetsky and Yaxley 2015). However, so far attention has focused on opx dissolution as a dominant process in kimberlite magma evolution and eruption from the base of the lithosphere, although this has not yet been validated through experiments at upper mantle

conditions (e.g., Stone and Luth 2016; Sokol et al. 2016), and could be reproduced only for a limited pressure range (Kamenetsky and Yaxley 2015). Here, we focus on the reaction of early high pressure kimberlite melt with clinopyroxene (cpx) and garnet (grt), manifest as solidified melt inclusions within kimberlite-hosted xenocrysts from the Lac de Gras kimberlite field (including the Diavik and Ekati diamond mines). Using reconstructed bulk compositions of these inclusions that trace extensive reaction with the host xenocrysts, we try to further constrain the possible nature of kimberlite melt at depth. Most importantly, we present evidence for reactions between the ascending melt and mantle minerals that lead to the eventual low pressure calcite-dominated mineralogy of kimberlites emplaced in the crust.

Polymineralic Inclusions in Kimberlite Xenocrysts

This study focuses on polymineralic inclusions (composed of multiple discrete mineral phases) that represent crystallized melt inclusions trapped in kimberlite megacryst phases (cpx and grt). Such polymineralic inclusions, also referred to as "spheroids" or "globules", have been reported to occur in a range of different megacryst minerals from kimberlites in different localities worldwide since the mid 1970s. Commonly reported phases in such inclusions are: phlogopite, olivine, carbonates (dominantly calcite), spinel, and serpentine. Haggerty and Boyd (1975) first described polymineralic inclusions in olivine megacrysts from the Monastery kimberlite in South Africa and interpreted them as early kimberlite melt with an immiscible sulphide liquid. Schulze (1985), studying inclusions in grt and cpx megacrysts, adopted this interpretation and extended it to propose that the trapped kimberlite melt may also constitute the magma from which the hosts crystallized. More recent studies of melt inclusions in Cr-diopside from the Diavik Diamond Mine in the Slave Craton, Canada, established a link to carbonatitic melts not in equilibrium with the host phases (van Achterbergh et al. 2002). In follow-up studies on the same samples, melt differentiation towards more silicate-rich melts was proposed, based on the observation of two end-member types of inclusions; carbonate-rich and more silicate-rich (van Achterbergh et al. 2004). Araújo *et al.* (2009) challenged the need for different inclusion end-members and stated that the spectrum of melt inclusions could "have formed through melt differentiation after

wall–rock interaction and fractionation from melts with kimberlitic composition". The presence of pure calcite in the inclusions has previously been attributed to disequilibrium unmixing and quenching in the final stages of kimberlite emplacement (van Achterbergh et al. 2004). Pivin et al. (2009) reported similar polymineralic inclusions within grt megacrysts in kimberlites from the Democratic Republic of Congo, and tentatively interpreted them as products of destabilization of an unknown original phase due to metasomatism.

Geological Setting

The Archean Slave Craton forms the north-western part of the Canadian Shield and is exposed in the Northwest Territories and Nunavut (e.g., Kusky 1989; Padgham 1992). The Slave Craton formed by tectonic accretion of a pre-3 Ga nucleus in the west to a Neoarchean juvenile arc in the east, creating a north-south trending suture (e.g., Davis et al. 1996). Collisional events in the Paleoproterozoic led to the formation of the Thelon-Taltson and Wopmay orogens that now partially surround the craton (e.g., Isachsen and Bowring 1994). The Slave Craton hosts multiple kimberlite fields with various emplacement ages ranging from Cambrian to Eocene (e.g., Creaser et al. 2004; Heaman et al. 2004). The central Lac de Gras (LDG) kimberlite field, which contains the Diavik and Ekati diamond mines, was principally active from 75 to 45 Ma (Cretaceous to Eocene) (Sarkar et al. 2015).

The LDG field is located east of the inferred craton suture (Fig. 1). Its kimberlite pipes define a 100 km by 200 km northwest-trending zone (Lockhart et al. 2004). The generally small pipes (2-12 ha surface area) intrude into metamorphosed Archean basement rock and are overlain by Quaternary glacial deposits (Fedortchouk and Canil 2004; Nowicki et al. 2004). For a detailed description of Diavik and Ekati kimberlites, the reader is referred to Moss et al. (2008) and Nowicki et al. (2004), respectively. The geochemistry of the LDG kimberlite field has been discussed in detail by Kjarsgaard et al. (2009). We studied inclusion-bearing xenocrysts from the Diavik and Ekati kimberlites (Fig. 1), where Cr-diopside hosted polymineralic inclusions are common.

Analytical Methods

Polished thin sections of megacrysts, some with surrounding kimberlite, were prepared avoiding the use of water, to prevent the dissolution of inclusion material. Samples with abundant and well-preserved inclusions were selected for imaging in back-scattered electron (BSE) mode using a scanning electron microscope (SEM) in the Canadian Centre for Isotopic Microanalysis (CCIM).

Major and minor element analyses of megacrysts and inclusion phases were collected in multiple analytical sessions by wavelength dispersive X-ray spectroscopy (WDS) using a JEOL 8900 electron probe microanalyzer (EPMA) at the University of Alberta. Analytical conditions and secondary standard results for the different minerals are given in Supplementary Data (Table S1). Trace element analyses for phlogopite were obtained by laser inductively coupled plasma mass spectrometry (LA-ICP-MS) at the CCIM Arctic Resources Laboratory, University of Alberta, using a RESOlution 193 nm ArF excimer laser ablation system coupled to a Thermo Scientific ELEMENT XR 2 mass spectrometer. Measuring conditions and secondary standard results are given in Supplementary Data (Table S1). LA-ICP-MS data reduction was performed using the Iolite software (Paton et al. 2011).

To obtain modal compositions of the inclusions, six megacrysts of cpx and seven of grt from the Point lake kimberlite, Ekati, were selected for automated mineralogical analysis using QEMSCAN® at the Universidad Católica del Norte, Chile. A detailed description of this technique is given in Ayling *et al.* (2011) and the operating conditions for these analyses were similar to those in Menzies et al. (2015). EPMA compositions were used in the elemental bulk calculations using mass balance.

Strontium isotopes were measured by thermal ionization mass spectrometry (TIMS) at the CCIM Arctic Resources Laboratory using a Thermo Scientific TRITON-Plus mass spectrometer. Carbonates in the inclusions were dissolved directly with 6N HCl. Host megacrysts were crushed and clear fragments were picked, undergoing two cleaning cycles (in 6N HCl at 120°C overnight, and rinsed in MQ water). The crystal fragments were dissolved in a mixture of HF and HNO_3. Column chemistry procedures to separate

Sr from other potentially interfering elements are described by Sarkar *et al.*, (2015). A drop of H_3PO_4 was added to the sample solution before drying down at 90 °C. $TaCl_5$ was added as an activator to the sample solution, which was then loaded to Re filaments. Two analyses of the NBS987 standard yielded a $^{87}Sr/^{86}Sr$ ratio of 0.71027 with a standard error of 0.00001. No corrections were made to the measured data.

Results

Megacryst Hosts

The cpx and grt samples in this study commonly exceed 1 cm in size and thus are megacrysts in a non-genetic sense (Mitchell 1986).

Cpx megacrysts were collected directly from drill core at the Diavik Diamond Mine. The host kimberlite is coherent (hypabyssal) kimberlite from the A154-North pipe containing abundant fresh olivine, plus ilmenite and grt megacrysts, and calcite of different textural populations. The cpx megacrysts are generally veined/fractured but often contain zones where the cpx has a fresh, clear appearance (Fig. 2a-c). Some cpx megacrysts show signs of post-emplacement reaction with the host kimberlite in the form of embayments or reaction rinds (brownish discoloration of the surrounding kimberlite, Fig. 2a). Calcite segregations within the host kimberlite were often observed in direct contact with cpx megacrysts (Fig. 2b). Four cpx megacrysts (> 2 cm in size) containing abundant inclusions were selected for further analysis.

Diavik grt samples were obtained from ~1 cm mineral concentrates (Fig. 2e). Their original spatial relationship to the kimberlite is unclear, however, some grains have attached remnants of the host kimberlite (kimberlite rinds). Grt crystals in this study have different genetic origins, as suggested by a color range from orange (eclogitic or low-Cr megacrystic) to red (lherzolitic or high-Cr megacrystic) and purple (harzburgitic) (Fig. 2e) (McLean et al. 2007). Polymineralic inclusions are most common in red grt grains (lherzolitic or high-Cr megacrystic). A total of 14 separate grt grains with inclusions were analyzed.

Megacryst minerals from the Point lake and Wolverine kimberlite pipes, located on the Ekati Mine claim block, were also examined. Both cpx and grt were obtained from mineral concentrates (> 6 mm) and are likely to represent fragments of even larger crystals. A total of nine cpx grains and 17 grt grains from Point Lake were found to contain inclusions. From the Wolverine sample suite, three cpx grains and six grt grains with inclusions were selected.

Classification and Thermobarometry

The majority of the cpx and grt mineral hosts to the polymineralic inclusions classify as Cr-diopside and Cr-pyrope, respectively (see Supplementary Table S2 for EPMA analyses). Their Cr-rich compositions may suggest a genetic link to the Cr-rich megacryst suite, first documented by Eggler *et al.* (1979). To obtain P-T estimates of equilibration for Cr-diopside megacrysts, the single cpx thermobarometer of Nimis and Taylor (2000) was used in combination with the compositional filters suggested by Grütter (2009). This exercise yielded temperatures averaging around 1015°C and pressures around 4.6 GPa (Table 1).

Polymineralic Inclusions

Polymineralic inclusions can be very abundant, especially in cpx, with up to 10 inclusions observed in single sample sections (Fig. 2c) (see also van Achterbergh et al. 2002; 2004). In total, 80 polymineralic inclusions have been found and imaged in 20 cpx grains, and 51 inclusions in 29 grt grains. Polymineralic inclusions are usually rounded and up to 2 mm in diameter (Fig. 2). Depending on whether their mineralogy is carbonate- or silicate-rich, they appear brownish-white or dark in thin section. The inclusions are generally located where veins/fractures with abundant fluid inclusions converge in the host grain (Fig. 2d, f). Optical microscopy and preliminary Raman spectroscopy indicate that the fluid inclusions are CO_2-rich (Gleeson, S.A., pers. comm.). Larger inclusions along these trails are often filled by phlogopite, calcite, and/or serpentine indicating that the veins are genetically related to the polymineralic inclusions (Fig. 2d, f). Hence, the polymineralic inclusions strictly are secondary in nature, as defined by Roedder (1984). However, although the veins occasionally connect to the host kimberlite

(where preserved) the appearance of polymineralic inclusions and kimberlite is markedly different (Fig. 2f). Some megacryst grains contain dark blebs close to grain edges that are in direct contact with the host kimberlite (Fig 2b). On the basis of similar mineralogy to the host kimberlite groundmass, the blebs most likely represent late-stage kimberlite melt that infiltrated the grain rims.

It is important to distinguish polymineralic inclusions from other mineral inclusions. For example, cpx megacrysts can contain rounded inclusions of fresh olivine. In grt crystals (especially purple grains) mineral inclusions of olivine are common but often pervasively altered (Fig. 2e). The resulting alteration assemblage is remnant olivine, with serpentine, calcite, and Ni-rich sulphide (vaesite or pentlandite). The proportion of secondary calcite that replaces olivine can exceed 50%, so that altered olivine inclusions in grt can be mistaken for carbonate-rich polymineralic inclusions (described below).

Mineralogy of Inclusions in Clinopyroxene

Polymineralic inclusions in cpx are commonly surrounded by a reaction rim containing abundant micro-inclusions (Fig. 3a-c). EPMA element distribution maps (Fig. 4) show that these rims are enriched in Ca, and depleted in Al and Na (also see Fig. 9). The maps further highlight the presence of phlogopite, calcite, and serpentine in the micro-inclusions. Inside polymineralic inclusions, common phases are calcite, phlogopite, serpentine/chlorite, olivine, and chromite (Fig. 3a-c). Two end-member inclusion types are distinguished based on the groundmass mineralogy of the inclusions. The groundmass can be composed entirely of calcite, which may display bright and dark zones in BSE images (Fig. 3a). Alternatively, the groundmass is comprised of hydrated Mg-Fe-silicates (serpentine or chlorite) often with a distinctive vermicular texture (Fig. 3c). In such inclusions calcite appears as small euhedral crystals or as blebs. In intermediate inclusions calcite can have a colloform texture (Fig. 3b). Based on the observation that inclusions may either contain a calcite-rich or a serpentine/chlorite-rich groundmass, a division into ‘carbonate-rich’ and ‘silicate-rich’ inclusions, as proposed by van Achterbergh et al. (2004), is justified.

Mineralogy of Inclusions in Garnet

Phases observed in polymineralic inclusions in grt megacrysts are the same as those within cpx megacrysts, but further include Al-rich cpx, Al-spinel, and Ni-sulphides (vaesite or pentlandite) (Fig. 3d-f). Al-spinels can have chromite cores, evident in BSE images as bright inner zones. Phlogopite crystals commonly line the inclusion walls. Importantly, carbonates within polymineralic inclusions in grt can be more Mg-rich (dolomite and Mg-calcite) as well as calcite (Fig. 3e). Alteration rims showing an enrichment/depletion of the host grt around inclusions are absent. Instead, inclusions are surrounded by grt dissolution features akin to kelyphite rims usually observed at the grt-kimberlite interface (e.g., Canil and Fedortchouk 1999). Analyzing these kelyphite zones using energy dispersive X-ray spectroscopy (EDS) with a defocused electron beam yielded similar spectra to those of pristine grt. Both silicate-rich and carbonate-rich groundmasses are present, the latter being less frequent. Hence, a distinction into 'carbonate-rich' and 'silicate-rich' end-members also seems practical for polymineralic inclusions in grt megacrysts.

Polymineralic inclusions in both host phases can contain accessory apatite and sulfides. Representative QEMSCAN® maps of the end-member inclusion types in Cr-diopside and Cr-pyrope are shown in Supplementary Figure 1.

Mineral Chemistry of Inclusion Phases

Olivine

Within polymineralic inclusions from both Cr-diopside and Cr-pyrope megacrysts, olivine appears as typically euhedral, oblate to elongate crystals comprising up to 25% of the inclusion area. Individual olivine crystals are compositionally homogenous, whereas significant compositional variation can be observed among different inclusions (Supplementary Table S3). Olivine also occurs as single-phase mineral inclusions in some Cr-pyrope and in Cr-diopside megacrysts. For comparison, olivine in kimberlite rinds attached to megacryst hosts was also analyzed.

Olivine compositions from polymineralic inclusions and as mineral inclusions in grt and cpx are compared to LDG kimberlite olivine core and rim data (Fig. 5). The LDG kimberlitic olivine data can be divided into two main trends: 1) cores with high NiO (and low CaO) at variable Mg/(Mg+Fe) (Mg#), and 2) rims with decreasing NiO (and increasing CaO) at relatively constant Mg# (arrow in Fig. 5a) (e.g., Fedortchouk and Canil 2004; Brett et al. 2009; Bussweiler et al. 2015).

Olivines in kimberlite rinds attached to cpx and grt hosts plot along the expected trends for LDG kimberlite olivine. In contrast, olivines within the polymineralic inclusions are distinguished by lower NiO and higher MnO, CaO, and Cr_2O_3 contents with decreasing Mg# (Fig. 5). Olivines from polymineralic inclusions in Cr-pyrope megacrysts have lower NiO, CaO, and Cr_2O_3 and higher MnO compared to those in cpx megacrysts. Viewed together, olivines from inclusions in the two hosts define a trend of decreasing NiO and Mg# that diverges off the olivine rim trend in kimberlites (Fig. 5a). A similar trend has been documented for megacrystic olivine in kimberlites and attributed to crystallization from a magma at depth (Boyd 1974).

Single phase olivine inclusions all plot in the field for olivine from LDG peridotite xenoliths (Fig. 5d) and partially overlap with compositions of olivines included in diamond (Stachel et al. 2003; Donnelly et al. 2007). Thus, altered olivine mineral inclusions in grt megacrysts, which can mimic polymineralic inclusions in terms of mineralogy, are easily distinguished by the chemical composition of remnant olivine, for example by their high NiO and Mg#.

Phlogopite

Phlogopite (Supplementary Table S4) occurs in nearly all polymineralic inclusions, comprising up to 25% of the inclusion area within Cr-diopside, and up to 50% of the inclusion area in Cr-pyrope. Phlogopite is usually homogeneous, but crystals zoned in Cr_2O_3 are observed. Phlogopite also occurs as single-phase mineral inclusions, and as intergrowths with other mineral inclusions.

Major element compositions of phlogopite in polymineralic inclusions fall into the range of kimberlitic phlogopite, but define a more restricted window in Mg# space (0.85 - 0.94; Fig. 6a). Phlogopite in polymineralic inclusions is further distinguished by higher Cr_2O_3 and more restricted TiO_2. Such elevated Cr contents have been observed in phlogopite from the Snap Lake kimberlite, NWT (Kopylova et al. 2010). Importantly, compared to global carbonatite- and kimberlite-derived phlogopite compositions (Reguir et al. 2009), the phlogopite data from polymineralic inclusions fall into the kimberlite field (Fig. 6d), suggesting that the polymineralic inclusions considered to be 'carbonate-rich' are in fact also of kimberlitic lineage.

Compositional differences among phlogopite in polymineralic inclusions are controlled by the host crystal rather than kimberlite pipe or inclusion type; phlogopite in polymineralic inclusions in Cr-pyrope has higher Cr_2O_3 (up to 4.5 wt.%) and slightly lower Mg# (~0.90) than phlogopite in polymineralic inclusions in Cr-diopside (Fig. 6). Phlogopite in polymineralic inclusions in Cr-pyrope also has higher Al_2O_3 contents and extends to higher Na_2O (Supplementary Table S4). BaO contents in phlogopite are relatively low in inclusions from either host phases, usually < 0.5 wt.% (0.2 wt.% on average), but tend to be higher in inclusions in Cr-pyrope (up to ~1.4 wt.%) (Supplementary Table S4). Phlogopite as single mineral inclusions, as megacrystic intergrowths (with grt, olivine and diopside), or cores of zoned phlogopite have significantly lower Cr_2O_3 contents.

Halogen contents in phlogopite were generally low (mostly F < 0.5 wt.%, Cl < 0.1 wt.%) (Supplementary Table S4). The highest F concentration (0.86 wt.%) was measured in a phlogopite in a 'carbonate-rich' inclusion in Cr-diopside from Diavik. The highest Cl concentration (0.13 wt.%) was measured in a megacrystic phlogopite intergrown with Cr-pyrope from Diavik.

Giuliani et al. (2016) performed a detailed investigation of phlogopite from the Bulfontein kimberlite, South Africa. Compared to their compositional fields for groundmass phlogopite (late crystallization) and high Ti-Cr cores (crystallization at depth), the trace element composition of phlogopite in polymineralic

inclusions are low in Zr, Ba, and Mn while extending to Cr-rich compositions and are thus clearly more similar to phlogopite crystallizing at depth (Fig. 6d-f).

Carbonates

Carbonate forms the groundmass in 'carbonate-rich' end-member inclusions. In intermediate to 'silicate-rich' inclusions carbonate is present as distinct crystals with colloform texture, as blebs, or as euhedral phenocrysts. Compositional zoning, evident as darker and brighter areas in BSE images, is common. Most analyzed carbonates are calcite with < 1.0 wt.% MgO; rarely calcite contains up to 5.0 wt.% MgO (Supplementary Table S5). Within 'silicate-rich' inclusions in Cr-pyrope megacrysts, dolomite (up to ~22 wt.% MgO) is present. FeO contents are generally low in calcite (< 0.5 wt.%) but are higher in dolomite (up to ~4.5 wt.%).

All analyzed carbonates in polymineralic inclusions plot within the reported compositional range of kimberlitic carbonates in terms of Ca# (Ca/(Ca+Mg+Fe)) and SrO contents (e.g., Armstrong et al. 2004) (Fig. 7a). In polymineralic inclusions, calcite has generally low SrO (< 1.0 wt.%). Higher SrO concentrations are restricted to bright zones (in BSE images) in either the groundmass of 'carbonate-rich' inclusions in Cr-diopside or zoned single crystals in 'silicate-rich' inclusions in Cr-pyrope. Dolomite within inclusions in Cr-pyrope also has low SrO contents (< 0.5 wt.%) and thus overlaps dolomite compositions in kimberlite. Carbonates in polymineralic inclusions, especially in 'silicate-rich' inclusions in Cr-pyrope, extend to higher MnO contents than kimberlitic calcite (Fig. 7b).

Chromite and Spinel

Chromite occurs in all polymineralic inclusions, whereas Cr-rich Al-spinel only occurs in polymineralic inclusions in Cr-pyrope. No clear compositional differences were found between 'carbonate-rich' and 'silicate-rich' inclusions (Supplementary Table S6).

Kimberlite chromite data show a trend of decreasing Cr# and increasing Ti contents at relatively constant Fe# (Fe/(Fe+Mg)), which is referred to as "magmatic spinel trend 1" according to the terminology of

Mitchell (1986, 1995). The less common "magmatic trend 2" is characterized by Fe-enrichment prior to an increase in Ti contents, which has been tentatively attributed to preceding crystallization of phlogopite (Mitchell 1995).

Chromites in polymineralic inclusions classify as titanian-magnesian-chromite (TIMAC, Mitchell (1986)) and overlap core compositions of chromite found in the kimberlite groundmass (Fig. 8). Such chromites are characteristic for kimberlites and are not present in carbonatites (Mitchell 1986). Chromites in polymineralic inclusions generally lie at the beginning of the two differentiation trends (Fig. 8). Analyses of chromites in polymineralic inclusions in Cr-diopsides, and some analyses in Cr-pyropes, plot along the beginning of magmatic trend 2 (Fig. 8b). This Fe-enrichment is in accordance with the abundant presence of phlogopite in the polymineralic inclusions. Co-crystallization of olivine may also play a role in Mg-depletion, as evident in the olivine differentiation trend (Fig. 5a).

Cr-rich Al-spinels within inclusions in Cr-pyrope are characterized by low TiO_2 contents (usually < 2.0 wt.%). Such spinels have no counterpart in the groundmass of LDG kimberlites (Armstrong et al. 2004; Roeder and Schulze 2008). However, some Cr-rich Al-spinels were found to contain cores of chromite. Such zoned spinels may also be the cause for mixed analyses of relatively low Cr# and elevated TiO_2 contents (Fig. 8c).

Spinel in peridotitic mantle xenoliths (coarse spinel-grt peridotites from Jericho) overlaps spinel in polymineralic inclusions in Cr# vs. Fe# space but can be distinguished by lower TiO_2 (Kopylova et al. 1999).

Serpentine and Chlorite

Serpentine/chlorite (Supplementary Table S7) is present in most polymineralic inclusions. In 'carbonate-rich' inclusions, serpentine (Mg-rich) commonly replaces olivine, and chlorite (Al-bearing) replaces phlogopite. In 'silicate-rich' inclusions, an intergrowth of serpentine and chlorite forms the groundmass and can display a characteristic vermicular texture.

Serpentine in kimberlites is defined by a broad range in Mg# (~0.80 - 0.95) and mostly has low Al_2O_3 contents (< 1.0 wt.%). However, Al_2O_3 concentrations up to ~8.0 wt.% have been reported in the literature (e.g., Mitchell, 1986). Serpentine within inclusions in Cr-diopsides from LDG lies at the high-Mg# end and extends to Al_2O_3 contents of up to ~5.0 wt.%, whereas serpentine within polymineralic inclusions in Cr-pyrope can have even higher Al_2O_3 contents (up to ~9.0 wt.%) (Supplementary Fig.2). Serpentine associated with altered olivine inclusions in Cr-pyrope has intermediate Mg# and Al_2O_3 contents, and low Cr_2O_3 and TiO_2 contents.

Clinopyroxene in Polymineralic Inclusions

Cpx is only present in polymineralic inclusions within Cr-pyrope hosts and occurs exclusively in 'silicate-rich' inclusions. Cpx in polymineralic inclusions generally classifies as Al-rich, Cr-bearing augite and less commonly diopside (Supplementary Table S8). It is chemically distinct from the Cr-diopside megacrysts hosts and the modified cpx in the alteration rims around the polymineralic inclusions (Fig. 9). There is some compositional overlap between cpx in inclusions in Cr-pyrope and the global cpx megacryst trend, for example in Mg# and TiO_2 contents. However, cpx in inclusions is more enriched in Cr_2O_3, Al_2O_3, and CaO, and has significantly lower Na_2O contents than typical cpx megacrysts (Fig. 9). Most prominently, cpx in inclusions has higher MnO contents (clustering around 0.3 wt.%) than all other cpx populations (Fig. 9f).

Strontium Isotopes

Sr isotopes were measured for 'carbonate-rich' inclusions and their Cr-diopside and Cr-pyrope hosts. Because Rb concentrations were generally very low (commonly below detection limits), the measured ratios were not corrected for radiogenic ingrowth of Sr since kimberlite eruption.

Inclusions in Cr-diopside have $^{87}Sr/^{86}Sr$ ratios of 0.7049 to 0.7053, whereas inclusions in Cr-pyrope are more radiogenic (0.7061 to 0.7071; Fig. 10). If a previous analysis of carbonate-rich globules in Cr-diopside megacrysts by van Achterbergh et al. (2002) is included, there is overlap in the range of Sr

isotopic values of the inclusions in the two hosts. Compared to groundmass calcite from the Jos kimberlite, Somerset Island (Malarkey et al. 2010), signatures of 'carbonate-rich' inclusions in both host minerals are less radiogenic than those of late-stage kimberlitic calcite that is presumed to be affected by increased crustal contamination experienced by kimberlite melts during ascent plus subsequent low-T hydrothermal alteration. But there is overlap (Fig. 10) with a population of "early" kimberlitic calcite, interpreted to be the product of magmatic crystallization (Malarkey et al. 2010).

Except for the most radiogenic 'carbonate-rich' inclusion in Cr-pyrope, the Sr signatures of the inclusions overlap with those of LDG kimberlites (Tappe et al. 2013). The host kimberlite (Diavik A154) has the most radiogenic signature of all LDG kimberlites and is slightly more radiogenic (0.70619) than inclusions in Cr-diopsides. The relatively radiogenic character has been previously attributed to derivation from a fertile peridotite domain within an otherwise highly depleted domain in the convecting upper mantle (Tappe et al. 2013). However, since LDG kimberlite isotope ratios were obtained from bulk samples, their more radiogenic Sr may be influenced by sampling of late-stage crustal components. The latter scenario seems plausible, because Sr isotope signatures measured in LDG perovskites - an early crystallizing phase in kimberlites - are lower (~0.70424) and have a narrower range (Sarkar et al. 2015).

Importantly, the Sr isotope ratios of the LDG host megacrysts are significantly lower than those of their inclusions, indicating isotopic disequilibrium, as found also by van Achterbergh *et al.* (2002). In addition, it can be noted that the difference in Sr ratios between inclusion and host is smaller for Cr-diopside than for Cr-pyrope (Fig. 10).

Reconstructed Bulk Compositions of Polymineralic Inclusions

Major element bulk compositions of polymineralic inclusions were reconstructed using modal proportions obtained with QEMSCAN® or EPMA element maps and mineral compositions measured with EPMA. The overall uncertainty of the reconstructed bulk compositions is thus a function of 1) the uncertainty of the modal abundances and 2) the variability of the averaged mineral compositions used in the calculation.

For 1), we have adopted a universal relative uncertainty of 5%, noting that this may be lower for major phases and higher for accessory phases. For 2), we observe that relative standard deviations of multiple EPMA analyses of a given component (in a given phase and in a given inclusion) are up to 10%. This uncertainty may be lower for major components (such as MgO, FeO and SiO_2) and higher for minor components (such as Na_2O and SrO). Thus, we report a propagated overall uncertainty of ~11% for each component of the reconstructed bulk compositions (Table 2).

Oxide totals range from ~63 wt.% in 'carbonate-rich' inclusions to ~86 wt.% in 'silicate-rich' inclusions (Table 2). Low totals are attributed to major components that were not analyzed, such as CO_2 in carbonates and H_2O in phlogopite and serpentine. P_2O_5 and S hosted in accessory apatite and sulfides presumably have a minor effect on the bulk composition, as well.

Notably, reconstructed bulk compositions of the inclusions plot along nearly continuous trends rather than forming discrete clusters of 'carbonate-rich' and 'silicate-rich' end-members (Fig. 11). The calculated bulk compositions of 'carbonate-rich' inclusions (>50% modal calcite) in Cr-diopside consistently lie below the threshold of 20 wt.% SiO_2 required for the designation of "carbonatite" (Le Maitre et al. 2002), whereas 'silicate-rich' inclusions extend to SiO_2 contents of up to ~40 wt.%. CaO steeply decreases with increasing SiO_2 content (Fig. 11a) whereas MgO and FeO increase (Fig. 11b, c). Polymineralic inclusions in the two hosts display similar general trends, but inclusions in Cr-pyrope are significantly more enriched in the components FeO, Cr_2O_3, and Al_2O_3 (Fig. 11d), as expected from the mineral chemistry described in the previous sections.

The Mg#s of the reconstructed bulk compositions have a large range from 0.76 to 0.98 (Table 2). Inclusions hosted in cpx have a mean Mg# of 0.93, whereas inclusions in grt have lower Mg# averaging around 0.81. It should be noted that Mg# is highest in inclusions where a great proportion of high-Mg serpentine and phlogopite is exposed. Mg# thus appears to be easily skewed by a sampling or cross-section effect (see Discussion).

Discussion

Polymineralic Inclusions as Snapshots of Melt-Rock Reaction

Each polymineralic inclusion within Cr-diopside is surrounded by a halo of micro-inclusions of phlogopite and calcite within a matrix of recrystallized cpx depleted in the jadeite component (Fig. 4). We interpret this halo as a reaction rim between incoming melt and the original host phase. The textural and chemical character of these reaction rims is independent of whether the inclusion is of the 'carbonate-rich' or 'silicate-rich' type and is similar to the spongy rims commonly observed around the outside of cpx grains in mantle-derived xenoliths (Taylor and Neal 1989; Ionov 1998; Carpenter et al. 2002; Su et al. 2012; Lu et al. 2015). Similarly, Cr-pyropes display a kelyphitic reaction zone around polymineralic inclusions of both types. Kelyphite – typically as a fine-grained intergrowth of opx, spinel, olivine, phlogopite and glass – is a commonly observed product of reaction between kimberlite melt and grt xenocrysts (e.g., Canil and Fedortchouk 1999; Spetsius and Taylor 2002).

We interpret spongy textures in Cr-diopsides and kelyphite zones in Cr-pyrope as different textural representations of the same process, namely the reaction of a melt with mantle minerals during ascent. Thus, it seems likely that the original melt in the two different host minerals was the same, as previously suggested for polymineralic inclusions in cpx and grt megacrysts from Kentucky kimberlites (Schulze 1985).

New and published Sr isotopic data on the host megacrysts and inclusions support the reaction relationship deduced from textures (Fig. 10). The host megacrysts are less radiogenic than the carbonate within the polymineralic inclusions, but the range in Sr isotopic compositions of the inclusions trends towards their hosts. This trend is more evident for carbonate included within Cr-diopside, for which there are two possible explanations: 1) The reaction between melt and host scavenges more Sr from the Cr-diopside (usually containing ~200 ppm Sr) than from the Cr-pyrope (< 2 ppm Sr); 2) The reaction between melt and host Cr-diopside is stronger, as indicated by the presence of spongy rims around

polymineralic inclusions that can be > 100 µm wide (Fig. 2d, 3, 4) and possibly by reaction rims around the outside of single Cr-diopside megacrysts (Fig. 2a). Polymineralic inclusions in Cr-pyrope tend to be smaller and their kelyphite zones narrower, so that the volume of interaction is smaller. But both hosts record clear evidence of reaction with the invading melt.

Evidence for Decarbonation Reactions

Both textural and isotopic data indicate that the melt parental to the polymineralic inclusions has reacted with their mantle-derived hosts, with a potentially stronger reaction observed for Cr-diopsides. The possible driving factors behind these processes might lie in a suite of decarbonation reactions – reactions that release CO_2 – long suspected to occur during the ascent of kimberlites (e.g., Wyllie and Huang 1975; Eggler 1986). In addition to the commonly invoked reaction of melt with opx (enstatite + dolomite melt → forsterite + diopside + CO_2; "opx dissolution"), the decarbonation reaction involving diopside has the form:

diopside + dolomite (melt) → forsterite + calcite + CO_2,

(more general: diopside + L → forsterite + calcite +V)

This reaction is expected to occur at pressures < 2.5 GPa (Stone and Luth 2016; Stone 2016). Polymineralic inclusions in Cr-diopside appear to preserve direct evidence of this reaction, as their mineralogy is dominated by the presence of pure calcite and forsteritic olivine, while the abundant fluid inclusion trails extending outward from the polymineralic inclusions could be the result of the accompanying exsolution of CO_2. General exsolution of a vapor phase (if H_2O is included in the system) may further be responsible for the crystallization of phlogopite and serpentine inside polymineralic inclusions, and/or in the surrounding micro-inclusions (e.g., Fig. 4).

Polymineralic inclusions in Cr-pyrope also show evidence for extensive chemical interaction with the host (as evident from kelyphite zones), but commonly contain dolomite. As there is no experimental

evidence for an analogous reaction between dolomite melt and grt to produce calcite, it seems logical that the dolomite preserved in polymineralic inclusions in Cr-pyrope could be pristine in nature.

Process and Timing of Melt Entrapment

A likely process for entrapment of a melt in mantle minerals is described as "necking down" by Roedder (1984) and has been proposed in previous studies on polymineralic inclusions in megacrysts (Schulze 1985; van Achterbergh et al. 2002; van Achterbergh et al. 2004; Araújo et al. 2009). In this process, a melt enters the host crystal along fractures and cleavage planes by dissolution and recrystallization. Surface reduction then results in the entrapment of discrete inclusions that may coalesce to form larger, rounded inclusions. Hence, reaction and the production of new minerals are an integral part of the necking down process. This process of melt infiltration may be further aided by crack formation due to rapid decompression, as described for the formation of fractures in kimberlitic olivine lined with carbonate (Brett et al. 2015).

Thermobarometry of the host Cr-diopsides indicates that they equilibrated at pressures of 4 - 5 GPa (~130 - 160 km), deep in the lithospheric mantle (Table 1). The preservation of polymineralic inclusions and the striking compositional zoning around them, such as spongy rims in Cr-diopside, suggest that the melt infiltration occurred shortly prior to or during kimberlite ascent. Otherwise the compositional zoning would have equilibrated quickly at their original deep lithospheric mantle temperature conditions (e.g., Schulze 1985). Similarly, the fine-grained texture of the kelyphite zones around inclusions within Cr-pyrope documents a rapid process during kimberlite ascent. In fact, dissolution experiments of grt xenocrysts in kimberlite melt suggest that this process occurs on a time scale of minutes (Canil and Fedortchouk 1999). Moreover, the decarbonation reaction proposed to account for the calcite-olivine(-phlogopite) assemblage of the inclusions within Cr-diopsides should take place at pressures < 2.5 GPa, consistent with reaction during kimberlite ascent.

Compositional Link to the Transporting Kimberlite Magma

Detailed investigation of individual mineral phases within polymineralic inclusions has shown that their compositions are similar to those crystallizing from kimberlite magma. Moreover, the phase compositions lie at the beginning of kimberlite mineral differentiation trends, suggesting that an early stage of kimberlite melt was trapped at mantle pressures. Particularly the evolution of spinels along magmatic trend 2 of the kimberlite compositional array (Fig. 8), and olivines falling along the megacryst trend (Fig. 5), suggests that polymineralic inclusions in both Cr-diopsides and Cr-pyropes from LDG kimberlites represent snapshots of kimberlite melt reacting with the lithospheric mantle during ascent. This model is further supported by the clear difference in the trace element compositions of phlogopite within the polymineralic inclusions versus groundmass phlogopite typically found in kimberlite (Fig. 6d-f). The phlogopite within the inclusions shows a striking similarity to high Ti-Cr phlogopite zones interpreted to have crystallized at depth (Giuliani et al. 2016).

No significant differences in mineral compositions exist between 'carbonate-rich' and 'silicate-rich' inclusion types, or between samples from different kimberlite pipes. Instead, mineral compositions appear to be controlled mainly by reaction and equilibration with the host megacrysts. Extensive chemical exchange between the invading melt and the host megacrysts is evident from the enrichment of individual inclusion phases in components such as Cr_2O_3, Al_2O_3, FeO, and MnO, in relation to the chemical character of their hosts; i.e. greater enrichment of these elements in Cr-pyropes compared to Cr-diopsides. In Cr-pyropes, elemental exchange may even lead to the stabilization of additional phases that are not typical of kimberlite, such as Al-rich cpx and Al-spinel by Al exchange.

The continuous range of bulk compositions from 'carbonate-rich' to 'silicate-rich' inclusions (Fig. 11) led van Achterbergh et al. (2002) to propose separate origins for the two inclusion types. However, we posit that the range in inclusion mineralogy and hence bulk compositions can be explained by a combination of: 1) The way in which the inclusions are exposed during sectioning will lead to random sampling of an assemblage dominated by carbonate and silicates (olivine, phlogopite, etc.), yielding the nearly

continuous range in bulk compositions illustrated well by $CaO\text{-}SiO_2$ and $MgO\text{-}SiO_2$ relations (Fig. 11a, b). 2) Small-scale fractional crystallization of the melt in a small fixed volume will produce different compositions that are then exposed in two-dimensional sections. This can explain observations such as the two generations of calcite in the inclusions, with the later generation being more enriched in incompatible elements such as Sr (evident as bright zones in BSE images). 3) The polymineralic inclusions represent trapped melts at various stages of reaction and differentiation prior to entrapment. Evidence for differentiation of the melt prior to entrapment comes from the range of olivine compositions seen in different inclusions that define a typical igneous fractionation trend (Fig. 5), as documented originally in olivine megacrysts by Boyd (1974). Fractionation is also clearly evident in the range of spinel compositions (Fig. 8). Differentiation is likely to be associated with the progressive assimilation of mantle material, such as opx (Kamenetsky et al. 2008; Russell et al. 2012; Pilbeam et al. 2013; Brett et al. 2015) and cpx – as observed here.

Because bulk compositions are easily skewed by a combination of the above processes (in addition to reaction with the host), the Mg# of the reconstructed bulk compositions cannot be reliably compared to the expected range of Mg# for LDG kimberlite liquids (Canil and Bellis 2008). Instead, we think it is more instructive to examine the calculated melts in equilibrium with olivine inside the polymineralic inclusions. Using the equation by Canil and Bellis (2008) along with their lower and upper estimates for Kd_{FeMg} ol/liq (0.12 and 0.27) we arrive at average Mg# for all polymineralic inclusions of 0.50 and 0.69, respectively. Olivines within inclusions in cpx yield higher liquid Mg# (0.52 and 0.71, respectively) than those in inclusions in grt (0.47 and 0.66, respectively), as expected from the higher Mg# of the host cpx relative to grt. These estimates of liquid Mg# overlap those by Canil and Bellis (2008) for LDG kimberlites (mostly < 0.60) which we interpret as further evidence that the polymineralic inclusions in cpx and grt megacrysts are linked to the early evolutionary stage of the transporting kimberlite magma.

A Glimpse at Primary Kimberlite Melt?

The reconstructed bulk compositions of polymineralic inclusions in Cr-diopside fall along a distinct trend in CaO-SiO_2 and MgO-SiO_2 space, produced by a combination of the three mechanisms described above (cross-section effect, internal fractional crystallization, and melt differentiation prior to entrapment), which essentially describes a mixing line between the end-member inclusion phases calcite and olivine (Fig. 12). The compositions of polymineralic inclusions in Cr-pyrope generally also fall along this trend, although they are more enriched in SiO_2, FeO, Cr_2O_3, and Al_2O_3 due to equilibration with the host (Fig. 11c, d).

The clear evidence of reactions between melt and host crystals makes an *original melt* composition difficult to obtain. The only possible result, using the inclusions themselves, is to arrive at an estimate for the composition of the melt after it has experienced reaction with the host. This composition will, necessarily, be subject to large uncertainties. Based on the observation that inclusions within Cr-pyrope have been more influenced by later equilibration with the host and noting that the reconstructed bulk compositions represent random samples of melt compositions, we use the average of the range of bulk compositions of inclusions in Cr-diopsides to obtain an average bulk composition. The resulting composition, which represents a melt *after* reaction with the host, has ~22 wt.% SiO_2, ~24 wt.% CaO and ~15 wt% MgO (star symbol in Fig. 11, 12). This composition is compared to experimental melts and primary kimberlite magma estimates in order to explore possible precursor melts (Fig. 12).

Partial melts of carbonated peridotite produced in different experimental studies (at $T \leq 1500°C$) generally lie at lower SiO_2 contents. However, a correlation of SiO_2 with T is observed in these experiments, so that the high T (1500°C) runs, e.g., by Gudfinnsson and Presnall (2005), approach our estimate of the average melt composition. These experiments are ~500°C above the equilibration temperature of the Cr-diopside megacrysts (Table 1), which seems excessively high. Alternatively, the experimental melts can be shifted onto the polymineralic inclusion array by reaction with the host crystals. In Fig. 12, this is demonstrated with reaction vectors towards cpx and grt compositions extending from one possible primary composition

characterized by maximum overlap of the experimental fields at melting conditions of roughly 6 GPa and 1400°C (question mark in Fig. 12). The digestion of other mantle silicates, especially opx, causes a similar displacement and may have started before the melt became trapped in the Cr-diopside and Cr-pyrope hosts (Kamenetsky et al. 2008; Russell et al. 2012; Pilbeam et al. 2013; Brett et al. 2015). Recent experimental studies, using carbonatite compositions obtained from previous low-degree partial melting experiments on mantle peridotite, suggest that opx dissolution does not occur until the kimberlite magma reaches pressures < 3.5 GPa (Stone and Luth 2016, and references therein). An indication that opx dissolution may be an important process during final (< 100 km) ascent and phenocryst crystallization of kimberlite magma – as opposed to the melt trapped as inclusions in cpx and grt megacrysts – lies in the mineral chemistry of olivine: Whereas olivines within the polymineralic inclusions define a fractionation trend (Fig. 5a), phenocrystic rims on olivines in kimberlite show a characteristic trend of decreasing Ni at buffered Mg# (arrow in Fig 5a) which has previously been attributed to the effect of opx dissolution (e.g., Pilbeam et al. 2013; Bussweiler et al. 2015).

Previous estimates of primary or parent kimberlite magma obtained through whole rock considerations (Le Roex et al. 2003; Kjarsgaard et al. 2009) also plot along the trend of reconstructed bulk compositions of polymineralic inclusions (Fig. 12). Compared to our average bulk composition, they are characterized by lower CaO and higher MgO and SiO_2 contents, which may suggest that these magma compositions, as well, have experienced some degree of mantle assimilation.

While the polymineralic inclusions constitute snapshots of kimberlite melt reacting with mantle minerals during ascent, it is important to note that they do not represent the primary or protokimberlite melt. Evidence for such precursor melts to LDG kimberlites may be preserved as melt inclusions in phenocryst phases (Kamenetsky et al. 2013), or as fluid inclusions in fibrous diamonds (Klein-BenDavid et al. 2007; Weiss et al. 2015), or can be gleaned from isotopic studies (Tappe et al. 2013). Together with the occurrence of sublithospheric diamonds at LDG (e.g., Tappert et al. 2005) these studies point towards an asthenospheric origin of the protokimberlite. The generally SiO_2-poor and CaO-rich compositions of the

already reacted kimberlite melt, as represented by the now crystallized polymineralic inclusions, is consistent with suggestions of the carbonatite-like nature of the protokimberlite melt (e.g. Dawson 1971; Dawson and Hawthorne 1973; Russell et al. 2012; Kamenetsky and Yaxley 2015; Kamenetsky 2016).

General Role of Decarbonation Reactions in Producing Calcite-Bearing Kimberlites

Oxybarometry studies applied to cratonic grt peridotites have shown that the lithospheric mantle below the LDG kimberlite field of the central Slave Craton tends to be more oxidized than the mantle below other cratons (Creighton et al. 2010; Luth and Stachel 2014), especially in the pressure-range of 4.5 to 6 GPa (~140 – 180 km), corresponding roughly to the depth of formation of the host megacrysts (Table 1; Supplementary Fig. 3). This has been attributed to the oxidizing effects of carbonate-rich fluids/melts (e.g., Creighton et al. 2008). The result of this metasomatism is the oxidation of local zones in the mid- to lowermost lithosphere beneath the LDG kimberlite field to levels conducive to the stabilization of carbonate. The expected stable carbonate phase is Mg-rich in any four-phase peridotite assemblage, i.e. dolomite (e.g., Wyllie and Huang 1975; Dalton and Presnall 1998a) or magnesite at higher pressure (Brey et al. 1983), and the melt produced from such carbonated peridotites is always dolomitic in composition (e.g., Irving and Wyllie 1975; Brey et al. 2008). However, LDG kimberlites, and kimberlites globally, are mostly dominated by calcite (e.g., Skinner and Clement 1979; Armstrong et al. 2004), as are the early kimberlite melts trapped as polymineralic inclusions in LDG megacrysts.

The reactions illustrated by the polymineralic inclusions provide an explanation for this discrepancy between expected high pressure melt compositions produced from carbonated peridotite and the calcite-rich nature of kimberlites in general, via the decarbonation reaction:

$$\text{diopside} + \text{dolomite (melt)} \rightarrow \text{forsterite} + \text{calcite} + CO_2,$$

This reaction is expected to begin during kimberlite ascent at depths around 70 km based on experimental and theoretical constraints (Wyllie and Huang 1975; Stone and Luth 2016; Stone 2016). The reaction may continue up to kimberlite emplacement in the crust, as indicated by the presence of reaction rinds (often

containing calcite segregations) around single Cr-diopside megacrysts in their host kimberlite (Fig. 2a, b). The latter observation also indicates that the dolomite-diopside decarbonation reaction is not just relevant for melt differentiation within the limited volume of polymineralic inclusions, but affects the entire rising batch of kimberlite magma. The similarity of the phase composition variations present in the kimberlite melt inclusions with those observed in kimberlites emplaced in the crust, indicates that this process of melt-rock reaction is critical in producing the observed compositions and mineralogy of kimberlites worldwide. In this scheme, the resulting exsolution of a vapor phase during the proposed reaction may be responsible for the crystallization of phlogopite and serpentine in the inclusions (and in the host kimberlite), as water may be present in the original melt and will accumulate during reaction and crystallization. In addition to driving the evolution of a dolomitic to a calcitic kimberlite melt at pressures in the shallower portion of the lithospheric mantle, the reaction provides a means of further CO_2 exsolution, which is seen as an important process in driving kimberlite emplacement (e.g., Eggler 1986; Brey et al. 1991; Russell et al. 2012). The reaction could proceed as long as the kimberlite magma contains a dolomitic melt component that can react with disaggregated diopside (either as Cr-diopside megacrysts or from peridotite xenoliths). While the abundance of diopside in lithospheric peridotites is relatively low (~10%), the presence of lherzolites and discrete Cr-diopside megacrysts in kimberlites is ubiquitous, indicating the likelihood of this reaction occurring in any section of cratonic lithosphere.

A schematic illustration of the formation of polymineralic inclusions and the concomitant evolution of the host kimberlite is summarized in Fig. 13. In sequence, the process is envisioned as (1) the formation of a dolomitic silico-carbonatite melt via melting of carbonated peridotite, (2) initial reaction with lithospheric mantle and early high pressure CO_2 exsolution, (3) lower pressure reactions with lithospheric wall rocks that change the bulk composition and release more CO_2, producing calcite, (4) the emplacement in the crust of the evolved kimberlite with the calcite-bearing mineral assemblage. The widespread occurrence of polymineralic inclusions in kimberlite megacrysts from numerous cratons (Haggerty and Boyd 1975;

Schulze 1985; van Achterbergh et al. 2002; Pivin et al. 2009; Araújo et al. 2009) is evidence of the general applicability of this process to the evolution of kimberlites.

Conclusions

1. Lac de Gras Cr-diopside and Cr-pyrope megacrysts contain abundant, large (up to 2 mm) polymineralic inclusions formed by necking down of melts starting at lithospheric mantle depths. The megacrysts genetically are mantle xenocrysts with peridotitic chemical signatures. Geothermobarometry suggests that they originate from within the lithospheric mantle (~4.6 GPa, 1015°C).
2. There is clear textural and isotopic evidence for disequilibrium between the host crystals and their polymineralic inclusions, the preservation of which establishes a temporal link to the kimberlite eruption.
3. The inclusion phases are broadly characteristic of kimberlite, with their compositions being overall consistent with the early stages of kimberlite differentiation trends. Enrichment of inclusion phases in components more abundant in the host crystals, such as Cr_2O_3 and Al_2O_3, points towards extensive reaction between inclusions and hosts. Trace element signatures of phlogopites within the inclusions constrain their crystallization from the melt inclusions at lithospheric mantle depths.
4. Although scattered by sectioning effects and reaction with the host phases, reconstructed bulk compositions of the inclusions bear a general resemblance to the experimentally derived partial melts of carbonated peridotites, if allowance is made for the assimilation of mantle minerals (including the host minerals cpx and grt). Thus, the polymineralic inclusions represent snapshots of kimberlite melt reacting with the lithospheric mantle during ascent.
5. Inclusions in Cr-diopside record direct evidence for a decarbonation reaction of the form: dolomitic melt + diopside → forsterite + calcite + CO_2, expected to begin at pressures < 2.5 GPa.

This reaction may play an important role in the en-route transformation of an upward moving dolomitic silico-carbonatite melt into the calcite-bearing kimberlite observed at the surface. As such, it is one of many reactions likely to occur between carbonatitic melt and lithospheric mantle that drive the chemical and volatile evolution in kimberlite.

Figure Captions

Fig. 1 Geological overview map of the Slave Craton indicating the location of major diamond mines, modified from Bleeker et al. (2004). Dashed line indicates inferred suture based on Pb isotopic studies (Davis et al. 1996).

Fig. 2 a) Section through kimberlite drill core exposing cpx megacryst with brownish reaction rind. b) Thin section of cpx megacryst in direct contact with calcite segregations in coherent (hypabyssal) kimberlite from the A154N pipe, Diavik. c) Thin section of cpx megacryst with abundant polymineralic inclusions and remnant host kimberlite ('kimberlite rind'). d) Photomicrograph of a polymineralic inclusion in cpx megacryst (courtesy of V.S. Kamenetsky). Polymineralic inclusions are typically located where fractures/veins with fluid inclusions converge and are typically surrounded by a thick reaction rim (spongy rim). e) Sample mount section of grt megacrysts from < 1 cm concentrates from Diavik. Color range indicates different origins. Polymineralic inclusions are most common in red grt grains (lherzolitic or megacrystic). f) Back-scattered electron (BSE) image of a polymineralic inclusion in a grt megacryst. Veins connect polymineralic inclusion to the host kimberlite, but mineralogy of inclusion and host kimberlite is markedly different.

Fig. 3 BSE images for polymineralic inclusions in Cr-diopside megacrysts (a-c) and in Cr-pyrope (grt) megacrysts (d-f). All inclusions in cpx are surrounded by spongy 'reaction rims', whereas inclusions in grt are surrounded by 'kelyphite zones'. a) 'Carbonate-rich' end-member inclusion with calcite (cc) groundmass composed of bright and dark zones, containing phlogopite (phl), olivine (ol), serpentine (srp), and chromite (chr). b) Intermediate inclusion with 'colloform' cc in Mg-Fe silicate groundmass, containing phl and chr. c) 'Silicate-rich' end-member inclusion with Mg-Fe-silicate groundmass composed of srp/chlorite (with distinctive vermicular texture), containing cc blebs and chr. d) 'Carbonate-rich' end-member inclusion with cc groundmass, containing phl, ol, srp, and chr. e) Intermediate inclusion with Mg-Fe silicate groundmass (vermicular texture) containing dolomite (dol), spinel (spl), and

cpx in addition to phl and chr. f) 'Silicate-rich' end-member inclusion with Mg-Fe-silicate groundmass containing cc as irregular blebs, phl, and chr.

Fig. 4 EPMA element distribution maps for Ca, Al, Na, Mg, K, and Sr of a polymineralic inclusion (intermediate type) in a cpx megacryst. Warmer colors indicate higher element concentrations. Reaction rims are enriched in Ca, and depleted in Al and Na. The maps highlight the presence of phlogopite (phl), calcite (cc), and serpentine (srp) in micro-inclusions around the main inclusion.

Fig. 5 Bivariate plots for olivine in polymineralic inclusions resolved by megacryst host (Cr-diopside and Cr-pyrope), and olivine in kimberlite rinds (a-c) and as mineral inclusions and intergrowths (d). Olivine was analyzed in eight polymineralic inclusions in Cr-diopside from Diavik and Point Lake (seven 'carbonate-rich', one 'silicate-rich'), and in four polymineralic inclusions in Cr-pyrope from Diavik (two 'carbonate-rich', two 'silicate-rich'). 12 olivine mineral inclusions were measured in Cr-pyropes from Diavik, one in Cr-pyrope from Point Lake, and one in Cr-diopside from Diavik. Reference data for LDG kimberlite olivines divided into cores and rims are from Brett et al. (2009) and Bussweiler et al. (2015). The arrow in (a) highlights the differentiation trend of phenocrystic rims (see text). Data of olivine inclusions in diamond from Lac de Gras, Slave Craton, Canada, are from Donnelly et al. (2007) and Stachel et al. (2003).

Fig. 6 A-C: Major element (EPMA data) bivariate plots for phlogopite in polymineralic inclusions resolved by megacryst host (Cr-diopside and Cr-pyrope). Phlogopite was analyzed in polymineralic inclusions in Cr-diopside from Diavik and Point Lake (five 'carbonate-rich', 19 'silicate-rich'), and in polymineralic inclusions in Cr-pyrope from Diavik, Point Lake, and Wolverine (four 'carbonate-rich', 29 'silicate-rich'). Reference data for phlogopite in kimberlites are from Eccles et al. (2004), Armstrong et al. (2004), and Kopylova et al. (2010). Mantle phlogopite data are from Menzies et al. (2004) and Giuliani et al. (2014). D-F: Trace element (LA-ICP-MS data) bivariate plots for phlogopite in polymineralic inclusions. The inset in D shows compositional fields for global carbonatite- and kimberlite-derived phlogopite (Reguir et al. 2009). Phlogopite in polymineralic inclusions clearly falls into the kimberlite

field. Compositional fields for groundmass phlogopite and high Ti-Cr phlogopite cores are based on data from Giuliani et al. (2016). Phlogopite in polymineralic inclusions is similar to the high Ti-Cr group (crystallized at depth) in many trace elements.

Fig. 7 Bivariate plots for carbonates resolved by megacryst host (Cr-diopside and Cr-pyrope). Carbonate was analyzed in polymineralic inclusions in Cr-diopside from Diavik (10 'carbonate-rich', 26 'silicate-rich'), Point Lake (four 'carbonate-rich', five 'silicate-rich'), and in polymineralic inclusions in Cr-pyrope from Diavik (two'carbonate-rich', nine 'silicate-rich') and Point Lake (three 'carbonate-rich', 11 'silicate-rich'). Carbonate was further analyzed in veins, kimberlite rinds, and altered olivine inclusions (in Cr-pyrope). Reference data for kimberlitic carbonate are from Armstrong et al. (2004).

Fig. 8 Bivariate plots for chromite/spinel in polymineralic inclusions resolved by megacryst host (Cr-diopside and Cr-pyrope) and in kimberlite rinds. Chromite/spinel was analyzed in inclusions in Cr-diopside from Diavik (six 'carbonate-rich', 21 'silicate-rich') and Point Lake (one 'silicate-rich'), and in inclusions in Cr-pyrope from Diavik (one 'carbonate-rich', 13 'silicate-rich'), Point Lake (one 'carbonate-rich', 19 'silicate-rich') and Wolverine (four 'silicate-rich'). In addition, chromite was analyzed in veins, kimberlite rinds, and around altered mineral inclusions. Reference data for spinel in LDG kimberlites are from Armstrong et al. (2004) and Roeder and Schulze (2008), for spinel in Jericho mantle xenoliths (peridotite/pyroxenite) from Kopylova et al. (1999). Shaded field represents magmatic spinel trend in kimberlitic chromites from Mitchell (1986).

Fig. 9 Bivariate plots for major and minor elements of cpx in polymineralic inclusions in Cr-pyrope. Data are compared against Cr-diopside hosts and spongy reaction rims (around polymineralic inclusions) from this study, and against megacrysts worldwide (Eggler et al. 1979; Hunter and Taylor 1984; de Bruin 2005; Pivin et al. 2009).

Fig. 10 $^{87}Sr/^{86}Sr$ ratios for 'carbonate-rich' inclusions and their Cr-diopside and Cr-pyrope hosts. Data points marked with * are previous analyses from van Achterbergh et al. (2002). Reference data for calcite

in the Jos kimberlite, Somerset Island, Nunavut, Canada are from Malarkey et al. (2010). LDG kimberlite whole rock data are from Tappe et al. (2013). LDG perovskite data are from Sarkar et al. (2015).

Fig. 11 Reconstructed bulk compositions of polymineralic inclusions resolved by megacryst host (Cr-diopside and Cr-pyrope). Inclusions in Cr-diopside are further resolved by end-member type based on carbonate-rich or silicate-rich groundmass. The star symbol represents an estimate of the average bulk composition as an average of all inclusions hosted in Cr-diopside (see Discussion).

Fig. 12 Schematic diagram relating the observed range of reconstructed bulk compositions of polymineralic inclusions (dashed, grey, double-arrow field) to partial melts of carbonated peridotite produced in high-P-T experiments, by reaction with the host phases Cr-diopside (cpx) and Cr-pyrope (grt), and to previous estimates of primary kimberlite magma based on whole rock geochemistry of hypabyssal kimberlites from Kimberley, South Africa (Le Roex et al. 2003) and from Lac de Gras (Kjarsgaard et al. 2009). Only experimental melts produced at T ≤1500°C are included in the fields, so that experimental conditions for the different melts are as follows, Gudfinnsson and Presnall (2005): 3.2-5.9 GPa, 1340-1500°C; Dalton and Presnall (1998a): 3-7 GPa, 1245-1430°C; Dalton and Presnall (1998b): 6 GPa, 1380-1480°; Brey et al. (2008): 6-10 GPa, 1300-1500°C; Foley et al. (2009): 4-6 GPa, 1090-1290°C.

Fig. 13 Schematic model of formation for polymineralic inclusions in Cr-diopside and Cr-pyrope megacrysts and the concomitant evolution of the host kimberlite. 1) Formation of a dolomitic silico-carbonatite melt via partial melting of carbonated peridotite close to the base of the lithosphere. 2) Ascending kimberlite melt infiltrates megacrysts after interaction with other mantle minerals (above 150 km) and is trapped by process of necking down (Roedder 1984) and/or decompression cracking (Brett et al. 2015). 3) Decarbonation reactions cause chemical exchange between inclusions and hosts during kimberlite ascent, forming spongy rims around inclusions in Cr-diopside, whereas kelyphite zones around inclusions in Cr-pyrope form by decompression reactions. In Cr-diopside, all Mg-carbonate is transformed to calcite, whereas primary dolomite may be preserved in inclusions in Cr-pyrope. Some

trails of fluid inclusions and veins form outwards due to the release of CO_2. Importantly, the reaction also occurs around the outside of the megacryst hosts, thereby releasing calcite and CO_2 into the transporting kimberlite. 4) Upon kimberlite emplacement globules have fully crystallized to polymineralic inclusions. 'Carbonate-rich' and 'silicate-rich' zones, formed by internal fractional crystallization within the inclusions, are exposed in two-dimensional sections and create the impression of compositional bimodality. Reaction rims and calcite segregations around Cr-diopsides and kelyphite rims around Cr-pyropes may suggest that they react with the host kimberlite until emplacement.

Supplementary Fig. 1 QEMSCAN® maps of polymineralic inclusions in Cr-diopside (a = PL_CPX_03 In01; b = PL_CPX_03 In10) and Cr-pyrope (c = PL_GRT_04 In13; d = PL_GRT_04 In05). Inclusions a) and c) are of the 'carbonate-rich', and b) and d) of the 'silicate-rich' end-member type. Modal proportions of the inclusions as obtained with QEMSCAN® are as follows: a) 10.3% ol; 11.4% srp; 11.2% phl; 65.8% cc; 0.1% ap. b) 4.0% ol; 60.4% srp; 16.5% phl; 15.2% cc; 0.1% ap. c) 8.2% ol; 0.2% cpx; 15.0% srp; 30.2% phl; 3.7% spl; 40.7% cc; 0.9% dol; 0.1% py. d) 0.8% ol; 2.0% cpx; 45.7% srp; 31.1% phl; 6.2% spl; 0.1% cc; 6.0% dol; 0.1% ap; 0.1% py. Mineral abbreviations are as follows: ol = olivine; cpx = clinopyroxene; srp = serpentine; phl = phlogopite; spl = spinel; cc = calcite; dol = dolomite; ap = apatite; py = pyrite.

Supplementary Fig. 2 Bivariate plots for major and minor elements in serpentine/chlorite in polymineralic inclusions resolved by megacryst host (Cr-diopside and Cr-pyrope) and in altered olivine mineral inclusions in Cr-pyrope. Reference data for kimberlitic serpentine are from Hayman et al. (2009) and Mitchell (1986).

Supplementary Fig. 3 ΔlogfO2 (FMQ) values for grt peridotites from different cratons (modified from Luth and Stachel 2014). Samples from the central Slave Craton (Creighton et al. 2010) are notably more oxidized than those from other cratons.

References

Araújo DP, Griffin WL, O'Reilly SY (2009) Mantle melts, metasomatism and diamond formation: Insights from melt inclusions in xenoliths from Diavik, Slave Craton. Lithos 112:675–682. doi: 10.1016/j.lithos.2009.06.005

Armstrong JP, Wilson M, Barnett RL, et al (2004) Mineralogy of primary carbonate-bearing hypabyssal kimberlite, Lac de Gras, Slave Province, Northwest Territories, Canada. Lithos 76:415–433. doi: 10.1016/j.lithos.2004.03.025

Ayling B, Rose P, Petty S (2011) Using QEMSCAN to Characterize Fracture Mineralization at the Newberry Volcano EGS Project, Oregon: A Pilot Study. GRC Trans 35:301–305.

Bleeker W, Ketchum J, Davis B, Sircombe K (2004) The Slave Craton From On Top: The Crustal View. courses.eas.ualberta.ca 1–5.

Boyd FR (1974) Olivine megacrysts from the kimberlites of Monastery and Frank Smith Mines, South Africa. Carnegie Inst Washingt Yearb 73 282–285.

Brett RC, Russell JK, Andrews GDM, Jones TJ (2015) The ascent of kimberlite: Insights from olivine. Earth Planet Sci Lett 424:119–131. doi: 10.1016/j.epsl.2015.05.024

Brett RC, Russell JK, Moss S (2009) Origin of olivine in kimberlite: Phenocryst or impostor? Lithos 112:201–212. doi: 10.1016/j.lithos.2009.04.030

Brey G, Brice WR, Ellis DJ, et al (1983) Pyroxene-carbonate reactions in the upper mantle. Earth Planet Sci Lett 62:63–74. doi: 10.1016/0012-821X(83)90071-7

Brey GP, Bulatov VK, Girnis a. V., Lahaye Y (2008) Experimental Melting of Carbonated Peridotite at 6-10 GPa. J Petrol 49:797–821. doi: 10.1093/petrology/egn002

Brey GP, Kogarko LN, Ryabchikov ID (1991) Carbon Dioxide in kimberlitic melts. Neues Jahrb für

Mineral Monatshefte 4:159–168.

Bussweiler Y, Foley SF, Prelević D, Jacob DE (2015) The olivine macrocryst problem: New insights from minor and trace element compositions of olivine from Lac de Gras kimberlites, Canada. Lithos 220-223:238–252. doi: 10.1016/j.lithos.2015.02.016

Canil D, Bellis AJ (2008) Phase equilibria in a volatile-free kimberlite at 0.1 MPa and the search for primary kimberlite magma. Lithos 105:111–117. doi: 10.1016/j.lithos.2008.02.011

Canil D, Fedortchouk Y (1999) Garnet dissolution and the emplacement of kimberlites. Earth Planet Sci Lett 167:227–237. doi: 10.1016/S0012-821X(99)00019-9

Carpenter RL, Edgar AD, Thibault Y (2002) Origin of spongy textures in clinopyroxene and spinel from mantle xenoliths, Hessian Depression, Germany. Mineral Petrol 74:149–162. doi: 10.1007/s007100200002

Creaser RA, Grütter H, Carlson J, Crawford B (2004) Macrocrystal phlogopite Rb–Sr dates for the Ekati property kimberlites, Slave Province, Canada: evidence for multiple intrusive episodes in the Paleocene and Eocene. Lithos 76:399–414. doi: 10.1016/j.lithos.2004.03.039

Creighton S, Stachel T, Eichenberg D, Luth RW (2010) Oxidation state of the lithospheric mantle beneath Diavik diamond mine, central Slave craton, NWT, Canada. Contrib to Mineral Petrol 159:645–657. doi: 10.1007/s00410-009-0446-x

Creighton S, Stachel T, McLean H, et al (2008) Diamondiferous peridotitic microxenoliths from the Diavik Diamond Mine, NT. Contrib to Mineral Petrol 155:541–554. doi: 10.1007/s00410-007-0257-x

Dalton J, Presnall D (1998a) Carbonatitic melts along the solidus of model lherzolite in the system CaO-MgO-Al2O3-SiO2-CO2 from 3 to 7 GPa. Contrib to Mineral Petrol 131:123–135.

Dalton JA, Presnall DC (1998b) The Continuum of Primary Carbonatitic – Kimberlitic Melt

Compositions in Equilibrium with Lherzolite : Data from at 6 GPa. J Petrol 39:1953–1964.

Davis W, Gariepy C, Breemen O Van (1996) Pb isotopic composition of late Archaean granites and the extent of recycling early Archaean crust in the Slave Province, northwest Canada. Chem Geol 130:255–269.

Dawson JB (1971) Advances in kimberlite geology. Earth Sci Rev 7:187–214. doi: 10.1016/0012-8252(71)90120-6

Dawson JB, Hawthorne JB (1973) Magmatic sedimentation and carbonatite differentiation in kimberlite sills at Benfontein, South Africa. J Geol Soc London 129:64–85.

de Bruin D (2005) Multiple compositional megacryst groups from the Uintjiesberg and Witberg kimberlites, South Africa. South African J Geol 108:233–246. doi: 10.2113/108.2.233

Donnelly CL, Stachel T, Creighton S, et al (2007) Diamonds and their mineral inclusions from the A154 South pipe, Diavik Diamond Mine, Northwest territories, Canada. Lithos 98:160–176. doi: 10.1016/j.lithos.2007.03.003

Eccles DR, Heaman LM, Luth RW, Creaser R a. (2004) Petrogenesis of the Late Cretaceous northern Alberta kimberlite province. Lithos 76:435–459. doi: 10.1016/j.lithos.2004.03.046

Eggler DH (1986) Kimberlites: How do they form? In: Kimberlites and Related Rocks. pp 489–504

Eggler DH, McCallum ME, Smith CB (1979) Megacryst assemblages in kimberlite from northern Colorado and southern Wyoming: Petrology, geothermometry-barometry and areal distribution. Boyd Meyer 2:213–226.

Fedortchouk Y, Canil D (2004) Intensive Variables in Kimberlite Magmas, Lac de Gras, Canada and Implications for Diamond Survival. J Petrol 45:1725–1745. doi: 10.1093/petrology/egh031

Foley SF, Yaxley GM, Rosenthal A, et al (2009) The composition of near-solidus melts of peridotite in

the presence of CO2 and H2O between 40 and 60 kbar. Lithos 112:274–283. doi: 10.1016/j.lithos.2009.03.020

Giuliani A, Phillips D, Kamenetsky VS, et al (2014) Petrogenesis of Mantle Polymict Breccias: Insights into Mantle Processes Coeval with Kimberlite Magmatism. J Petrol 55:831–858. doi: 10.1093/petrology/egu008

Giuliani A, Phillips D, Kamenetsky VS, Goemann K (2016) Constraints on kimberlite ascent mechanisms revealed by phlogopite compositions in kimberlites and mantle xenoliths. Lithos 240-243:189–201. doi: 10.1016/j.lithos.2015.11.013

Grütter HS (2009) Pyroxene xenocryst geotherms: Techniques and application. Lithos 112:1167–1178. doi: 10.1016/j.lithos.2009.03.023

Gudfinnsson GH, Presnall DC (2005) Continuous gradations among primary carbonatitic, kimberlitic, melilititic, basaltic, picritic, and komatiitic melts in equilibrium with garnet lherzolite at 3-8 GPa. J Petrol 46:1645–1659. doi: 10.1093/petrology/egi029

Haggerty SE, Boyd FR (1975) Kimberlite inclusions in an olivine megacryst from Monastery. In: Kimberlite Symposium. Cambridge,

Hayman PC, Cas RAF, Johnson M (2009) Characteristics and alteration origins of matrix minerals in volcaniclastic kimberlite of the Muskox pipe (Nunavut, Canada). Lithos 112:473–487. doi: 10.1016/j.lithos.2009.06.025

Heaman LM, Kjarsgaard BA, Creaser RA (2004) The temporal evolution of North American kimberlites. Lithos 76:377–397. doi: 10.1016/j.lithos.2004.03.047

Hunter RH, Taylor LA (1984) Magma-mixing in the low velocity zone: kimberlitic megacrysts from Fayette County, Pennsylvania. Am Mineral 69:16–29.

Ionov D (1998) Trace Element Composition of Mantle-derived Carbonates and Coexisting Phasesin

Peridotite Xenoliths from Alkali Basalts. J Petrol 39:1931–1941. doi: 10.1093/petroj/39.11-12.1931

Irving AJ, Wyllie PJ (1975) Subsolidus and melting relationships for calcite, magnesite and the join CaCO3-MgCO3 to 36 kb. Geochim Cosmochim Acta 39:35–53. doi: 10.1016/0016-7037(75)90183-0

Isachsen C, Bowring S (1994) Evolution of the Slave craton. Geology 22:917–920.

Kamenetsky VS (2016) Comment on: The ascent of kimberlite: Insights from olivine" authored by Brett R.C. et al. [Earth Planet. Sci. Lett. 424 (2015) 119–131]. Earth Planet Sci Lett 440:187–189. doi: 10.1016/j.epsl.2016.02.016

Kamenetsky VS, Grütter H, Kamenetsky MB, Gömann K (2013) Parental carbonatitic melt of the Koala kimberlite (Canada): Constraints from melt inclusions in olivine and Cr-spinel, and groundmass carbonate. Chem Geol 353:96–111. doi: 10.1016/j.chemgeo.2012.09.022

Kamenetsky VS, Kamenetsky MB, Golovin A V., et al (2012) Ultrafresh salty kimberlite of the Udachnaya–East pipe (Yakutia, Russia): A petrological oddity or fortuitous discovery? Lithos 152:173–186. doi: 10.1016/j.lithos.2012.04.032

Kamenetsky VS, Kamenetsky MB, Sobolev a. V., et al (2008) Olivine in the Udachnaya-East Kimberlite (Yakutia, Russia): Types, Compositions and Origins. J Petrol 49:823–839. doi: 10.1093/petrology/egm033

Kamenetsky VS, Yaxley GM (2015) Carbonate-silicate liquid immiscibility in the mantle propels kimberlite magma ascent. Geochim Cosmochim Acta 158:48–56. doi: 10.1016/j.gca.2015.03.004

Kjarsgaard BA, Pearson DG, Tappe S, et al (2009) Geochemistry of hypabyssal kimberlites from Lac de Gras, Canada: Comparisons to a global database and applications to the parent magma problem. Lithos 112:236–248. doi: 10.1016/j.lithos.2009.06.001

Klein-BenDavid O, Izraeli ES, Hauri E, Navon O (2007) Fluid inclusions in diamonds from the Diavik

mine, Canada and the evolution of diamond-forming fluids. Geochim Cosmochim Acta 71:723–744. doi: 10.1016/j.gca.2006.10.008

Kopylova MG, Matveev S, Raudsepp M (2007) Searching for parental kimberlite melt. Geochim Cosmochim Acta 71:3616–3629. doi: 10.1016/j.gca.2007.05.009

Kopylova MG, Mogg T, Smith BS (2010) Mineralogy of the Snap Lake kimberlite, Northwest Territories, Canada, and compositions of phlogopite as records of its crystallization. Can Mineral 48:549–570. doi: 10.3749/canmin.48.3.549

Kopylova MG, Russell JK, Cookenboo H (1999) Petrology of Peridotite and Pyroxenite Xenoliths from the Jericho Kimberlite: Implications for the Thermal State of the Mantle beneath the Slave Craton, Northern Canada. J Petrol 40:79–104. doi: 10.1093/petroj/40.1.79

Kusky T (1989) Accretion of the Archean Slave province. Geology 17:63–67.

Le Maitre RW, Streckeisen A, Zanettin B, et al (eds) (2002) Igneous Rocks: A Classification and Glossary of Terms. Cambridge University Press

Le Roex AP, Bell DR, Davis P (2003) Petrogenesis of Group I Kimberlites from Kimberley, South Africa: Evidence from Bulk-rock Geochemistry. J Petrol 44:2261–2286. doi: 10.1093/petrology/egg077

Lockhart G, Grütter H, Carlson J (2004) Temporal, geomagnetic and related attributes of kimberlite magmatism at Ekati, Northwest Territories, Canada. Lithos 77:665–682. doi: 10.1016/j.lithos.2004.03.029

Lu J, Zheng JP, Griffin WL, O'Reilly SY (2015) Microscale effects of melt infiltration into the lithospheric mantle : Peridotite xenoliths from Xilong , South China. Lithos 232:111–123. doi: 10.1016/j.lithos.2015.06.013

Luth RW, Stachel T (2014) The buffering capacity of lithospheric mantle: implications for diamond

formation. Contrib to Mineral Petrol 168:1083. doi: 10.1007/s00410-014-1083-6

Malarkey J, Pearson DG, Kjarsgaard BA, et al (2010) From source to crust: Tracing magmatic evolution in a kimberlite and a melilitite using microsample geochemistry. Earth Planet Sci Lett 299:80–90. doi: 10.1016/j.epsl.2010.08.020

McLean H, Banas A, Creighton S, et al (2007) Garnet xenocrysts from the Diavik mine, NWT, Canada: Composition, color, and paragenesis. Can Mineral 45:1131–1145. doi: 10.2113/gscanmin.45.5.1131

Menzies A, Alvarez E, Belmar M, et al (2015) Quantification of trace REE-minerals using automated mineralogy. In: Chilean Geological Congress, La Serena, Chile.

Menzies A, Westerlund K, Grütter H, et al (2004) Peridotitic mantle xenoliths from kimberlites on the Ekati Diamond Mine property, N.W.T., Canada: major element compositions and implications for the lithosphere beneath the central Slave craton☆. Lithos 77:395–412. doi: 10.1016/j.lithos.2004.04.013

Mitchell RH (1986) Kimberlites: Mineralogy, Geochemistry and Petrology. Plenum Press, New York

Mitchell RH (1995) Kimberlites, Orangeites, and Related Rocks. Plenum Press, New York

Moss S, Russell JK, Andrews GDM (2008) Progressive infilling of a kimberlite pipe at Diavik, Northwest Territories, Canada: Insights from volcanic facies architecture, textures, and granulometry. J Volcanol Geotherm Res 174:103–116. doi: 10.1016/j.jvolgeores.2007.12.020

Nielsen T, Sand K (2008) The Majuagaa kimberlite dike, Maniitsoq region, West Greenland: constraints on an Mg-rich silicocarbonatitic melt composition from groundmass mineralogy and bulk. Can Mineral 46:1043–1061.

Nimis P, Taylor WR (2000) Single clinopyroxene thermobarometry for garnet peridotites. Part I. Calibration and testing of a Cr-in-Cpx barometer and an enstatite-in-Cpx thermometer. Contrib to Mineral Petrol 139:541–554. doi: 10.1007/s004100000156

Nowicki T, Crawford B, Dyck D, et al (2004) The geology of kimberlite pipes of the Ekati property, Northwest Territories, Canada. Lithos 76:1–27. doi: 10.1016/j.lithos.2004.03.020

Padgham WA (1992) Mineral deposits in the Archean Slave Structural Province; lithological and tectonic setting. Precambrian Res 58:1–24.

Paton C, Hellstrom J, Paul B, et al (2011) Iolite: Freeware for the visualisation and processing of mass spectrometric data. J Anal At Spectrom 26:2508–2518. doi: 10.1039/c1ja10172b

Pilbeam LH, Nielsen TFD, Waight TE (2013) Digestion Fractional Crystallization (DFC): an Important Process in the Genesis of Kimberlites. Evidence from Olivine in the Majuagaa Kimberlite, Southern West Greenland. J Petrol. doi: 10.1093/petrology/egt016

Pivin M, Féménias O, Demaiffe D (2009) Metasomatic mantle origin for Mbuji-Mayi and Kundelungu garnet and clinopyroxene megacrysts (Democratic Republic of Congo). Lithos 112:951–960. doi: 10.1016/j.lithos.2009.03.050

Price SE, Russell JK, Kopylova MG (2000) Primitive magma from the Jericho Pipe, NWT, Canada: constraints on primary kimberlite melt chemistry. J Petrol 41:789–808.

Reguir EP, Chakhmouradian AR, Halden NM, et al (2009) Major- and trace-element compositional variation of phlogopite from kimberlites and carbonatites as a petrogenetic indicator. Lithos 112:372–384. doi: 10.1016/j.lithos.2009.05.023

Roedder E (1984) Fluid Inclusions, Volume 12. Mineralogical Society of America

Roeder PL, Schulze DJ (2008) Crystallization of groundmass spinel in kimberlite. J Petrol 49:1473–1495. doi: 10.1093/petrology/egn034

Russell JK, Porritt LA, Lavallée Y, Dingwell DB (2012) Kimberlite ascent by assimilation-fuelled buoyancy. Nature 481:352–6. doi: 10.1038/nature10740

Sarkar C, Heaman LM, Pearson DG (2015) Duration and periodicity of kimberlite volcanic activity in the Lac de Gras kimberlite field, Canada and some recommendations for kimberlite geochronology. Lithos 218-219:155–166. doi: 10.1016/j.lithos.2015.01.017

Schulze D (1985) Evidence for primary kimberlitic liquids in megacrysts from kimberlites in Kentucky, USA. J Geol 93:75–79.

Skinner E, Clement C (1979) Mineralogical classification of southern African kimberlites. In: Kimberlites, Diatremes, and Diamonds: Their Geology, Petrology, and Geochemistry. pp 129–139

Sokol AG, Kruk AN, Chebotarev DA, Palyanov YN (2016) Carbonatite melt–peridotite interaction at 5.5–7.0 GPa: Implications for metasomatism in lithospheric mantle. Lithos 248-251:66–79. doi: 10.1016/j.lithos.2016.01.013

Sparks RSJ, Brooker RA, Field M, et al (2009) The nature of erupting kimberlite melts. Lithos 112:429–438. doi: 10.1016/j.lithos.2009.05.032

Spetsius Z V., Taylor LA (2002) Partial Melting in Mantle Eclogite Xenoliths: Connections with Diamond Paragenesis. Int Geol Rev 44:973–987. doi: 10.2747/0020-6814.44.11.973

Stachel T, Harris JW, Tappert R, Brey GP (2003) Peridotitic diamonds from the Slave and the Kaapvaal cratons—similarities and differences based on a preliminary data set. Lithos 71:489–503. doi: 10.1016/S0024-4937(03)00127-0

Stone RS (2016) The behavior of orthopyroxene in carbonatitic melts. University of Alberta

Stone RS, Luth RW Orthopyroxene assimilation in potential primary kimberlite melts.

Su B-X, Zhang H-F, Deloule E, et al (2012) Extremely high Li and low δ7Li signatures in the lithospheric mantle. Chem Geol 292-293:149–157. doi: 10.1016/j.chemgeo.2011.11.023

Tappe S, Graham Pearson D, Kjarsgaard BA, et al (2013) Mantle transition zone input to kimberlite

magmatism near a subduction zone: Origin of anomalous Nd-Hf isotope systematics at Lac de Gras, Canada. Earth Planet Sci Lett 371-372:235–251. doi: 10.1016/j.epsl.2013.03.039

Tappert R, Stachel T, Harris JW, et al (2005) Mineral inclusions in diamonds from the Panda kimberlite, Slave Province, Canada. Eur J Mineral 17:423–440. doi: 10.1127/0935-1221/2005/0017-0423

Taylor LA, Neal CR (1989) Eclogites with Oceanic Crustal and Mantle Signatures from the Bellsbank Kimberlite , South Africa , Part I : Mineralogy , Petrography , and Whole Rock Chemistry Author (s): Lawrence A . Taylor and Clive R . Neal Published by : The University of Chicago. Group 97:551–567.

van Achterbergh E, Griffin WL, Ryan CG, et al (2002) Subduction signature for quenched carbonatites from the deep lithosphere. Geology 30:743. doi: 10.1130/0091-7613(2002)030<0743:SSFQCF>2.0.CO;2

van Achterbergh E, Griffin WL, Ryan CG, et al (2004) Melt inclusions from the deep Slave lithosphere: implications for the origin and evolution of mantle-derived carbonatite and kimberlite. Lithos 76:461–474. doi: 10.1016/j.lithos.2004.04.007

Weiss Y, McNeill J, Pearson DG, et al (2015) Highly saline fluids from a subducting slab as the source for fluid-rich diamonds. Nature 524:339–342. doi: 10.1038/nature14857

Wyllie PJ, Huang WL (1975) Peridotite, kimberlite, and carbonatite explained in the system CaO-MgO-SiO2-CO2. Geology 621–624.

Figure1

Click here to download Figure Fig1.jpg

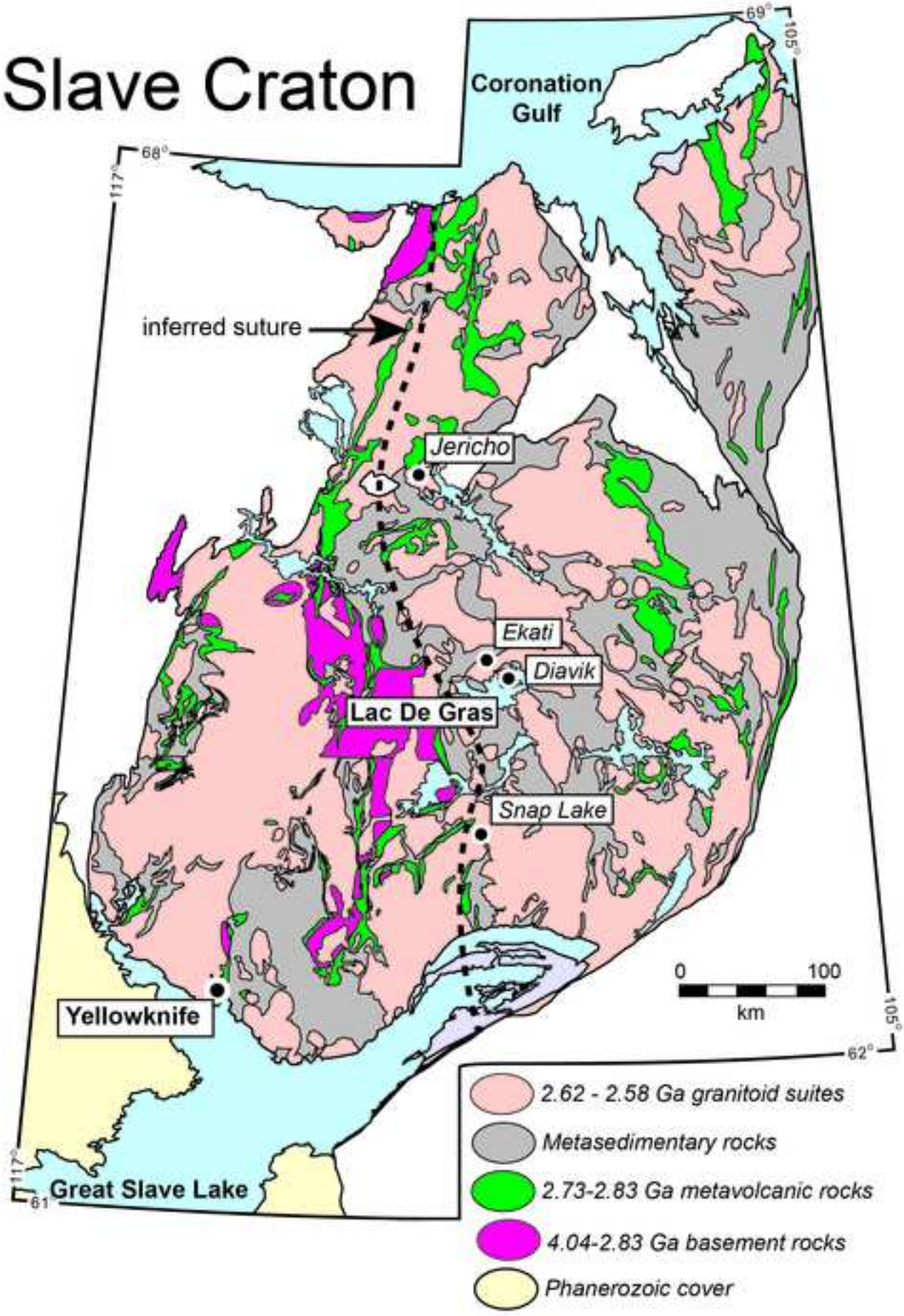

Figure2

Click here to download Figure Fig2.jpg

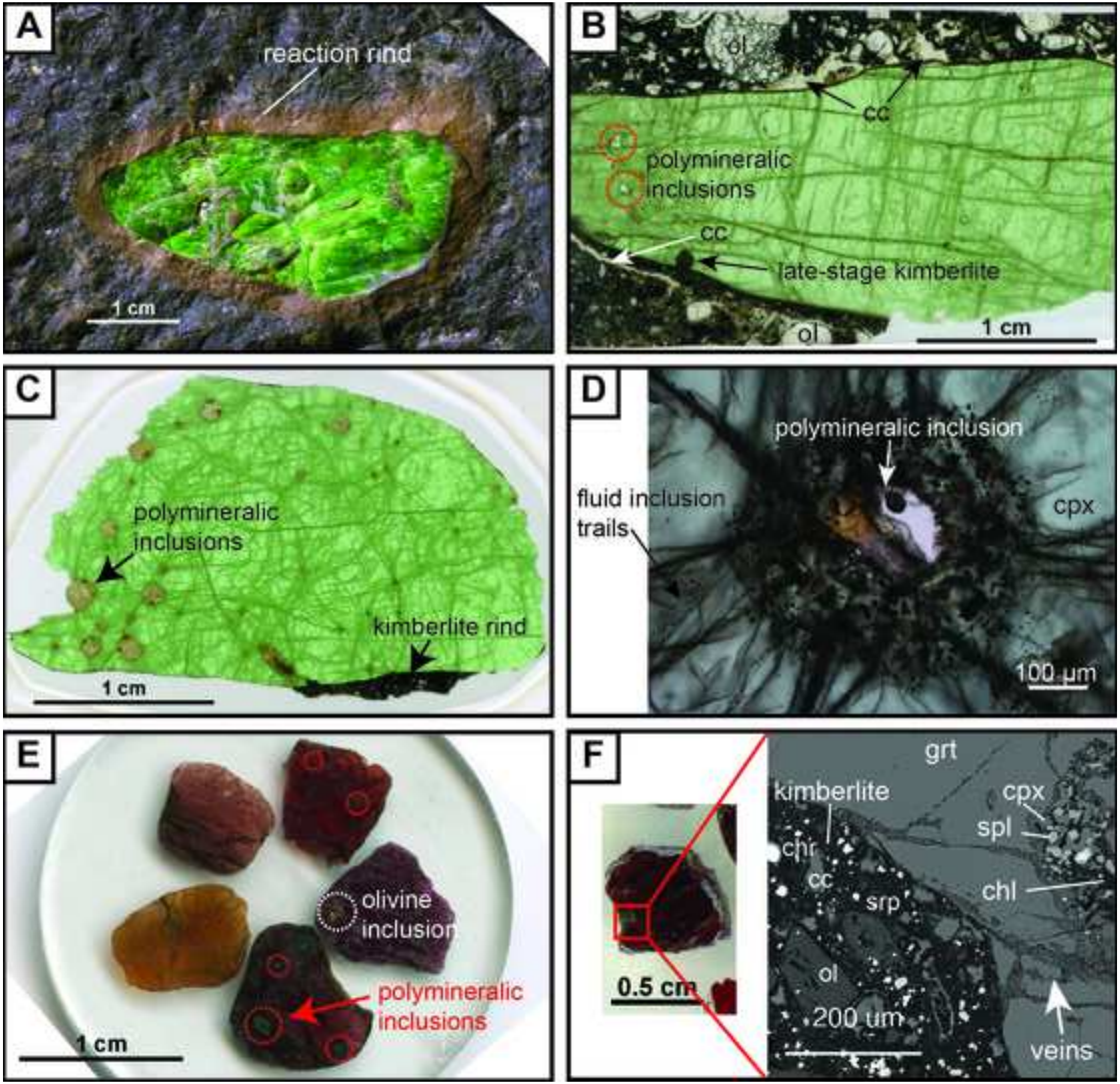

Figure3

Click here to download Figure Fig3.jpg

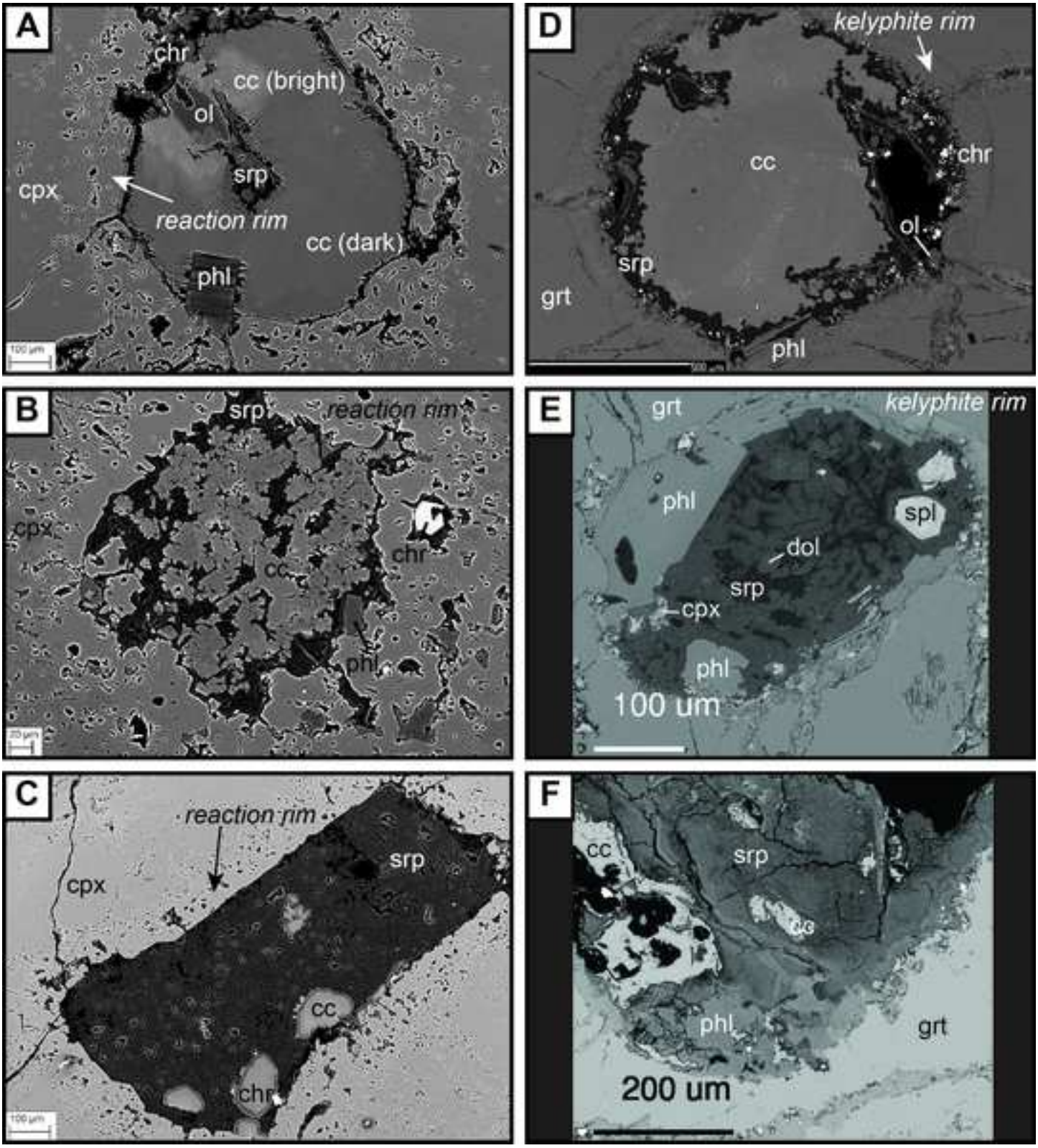

Figure4

Click here to download Figure Fig4.jpg

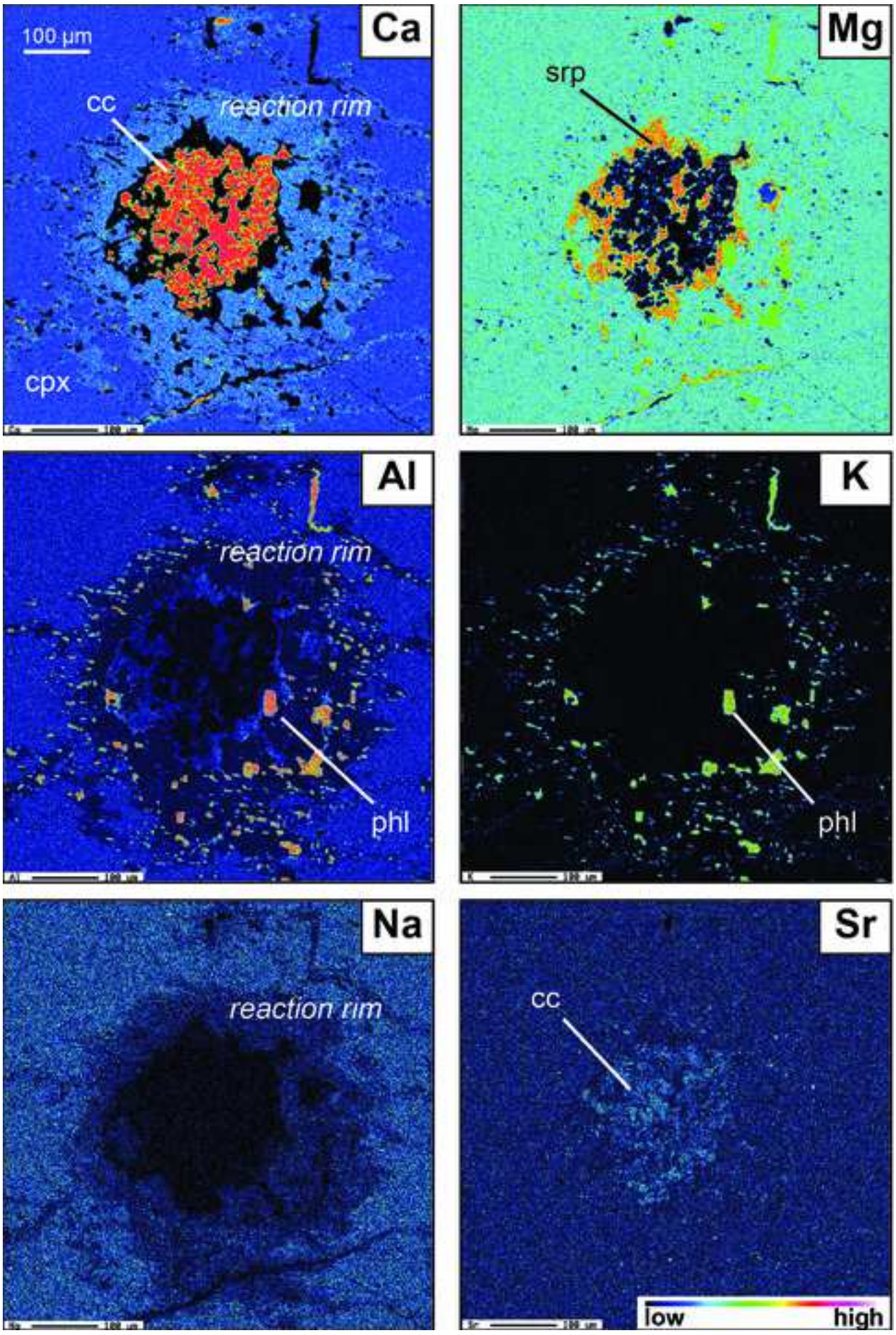

Figure5

Click here to download Figure Fig5.jpg

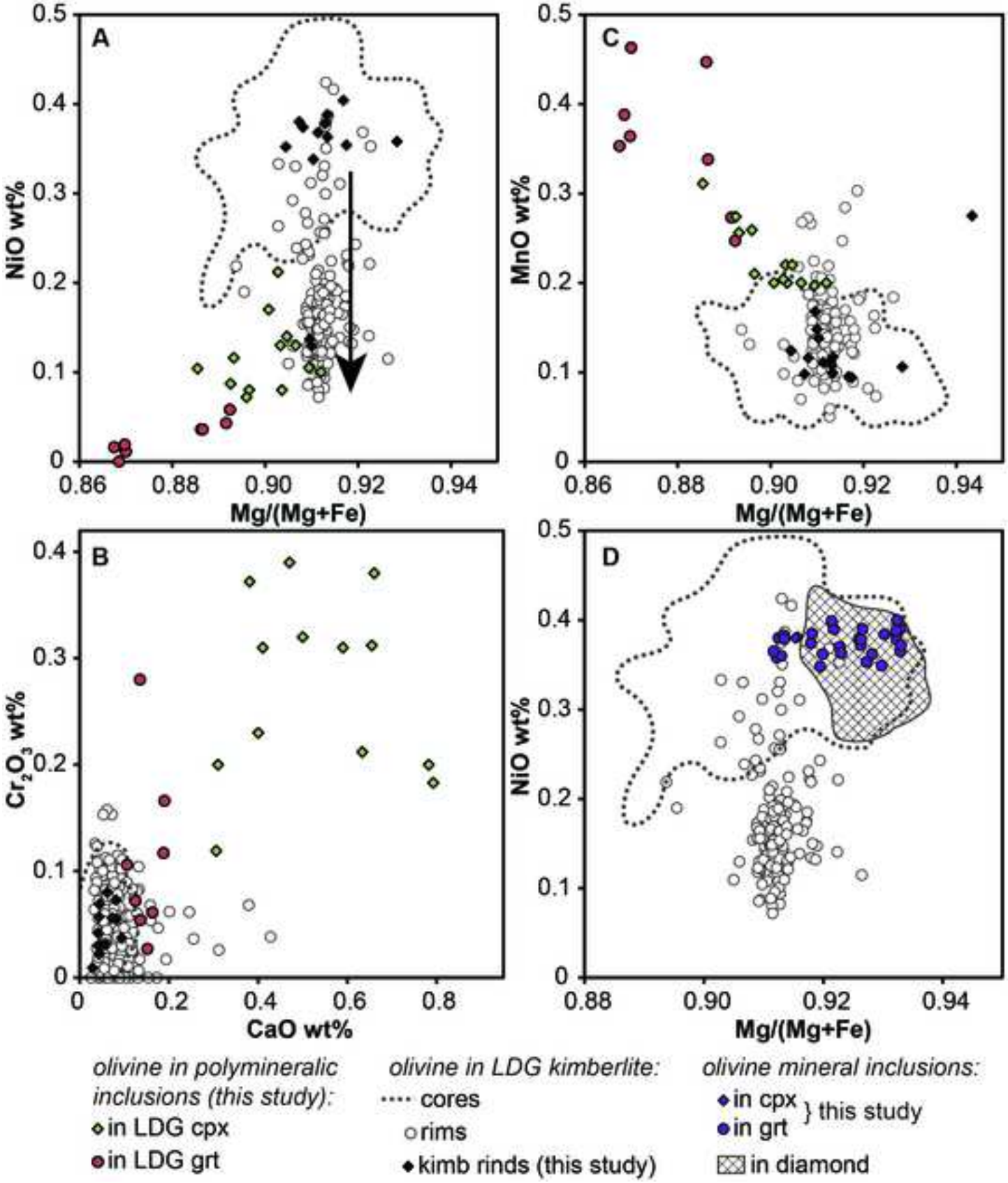

Figure6

Click here to download Figure Fig6.jpg

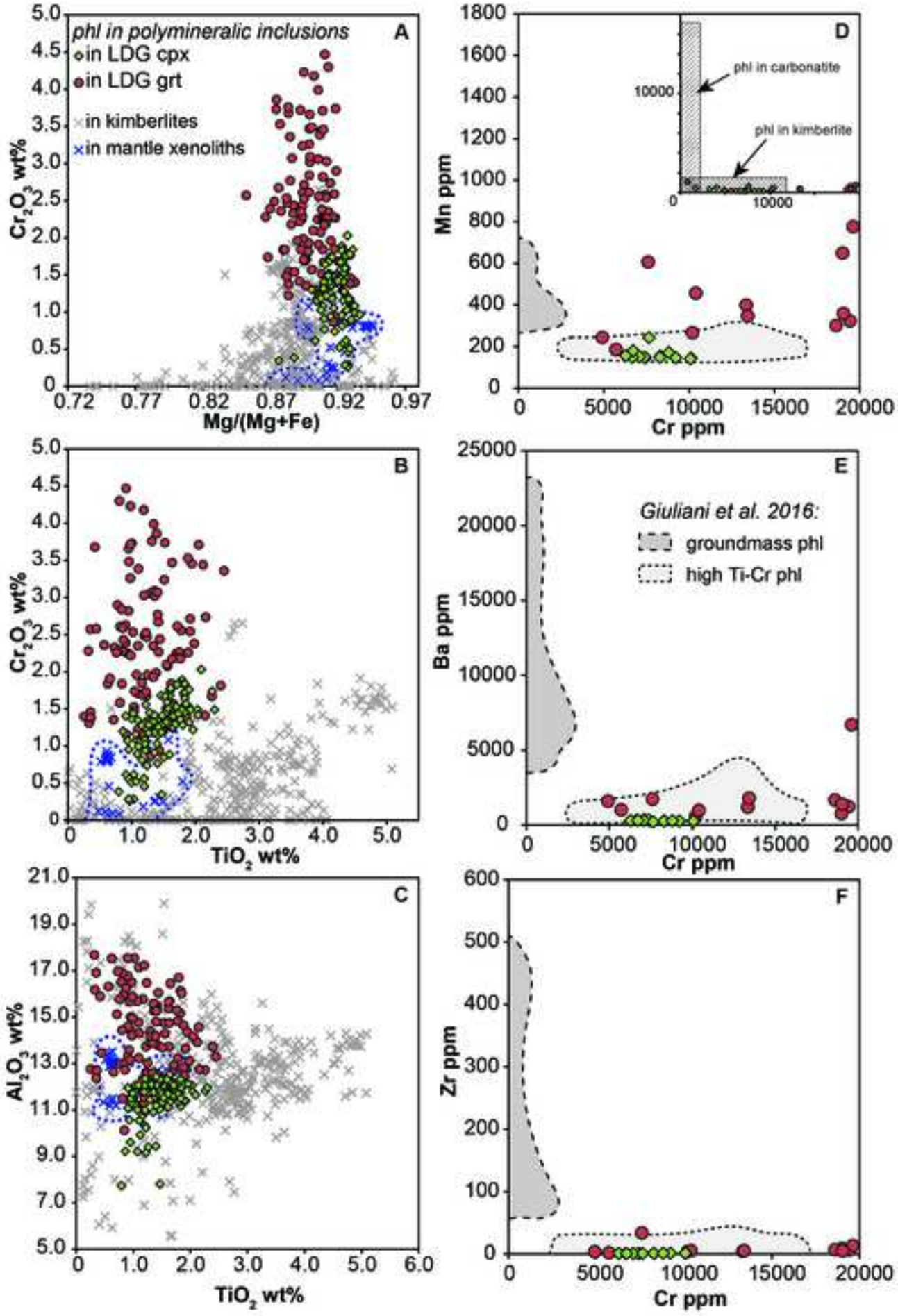

Figure7

Click here to download Figure Fig7.jpg

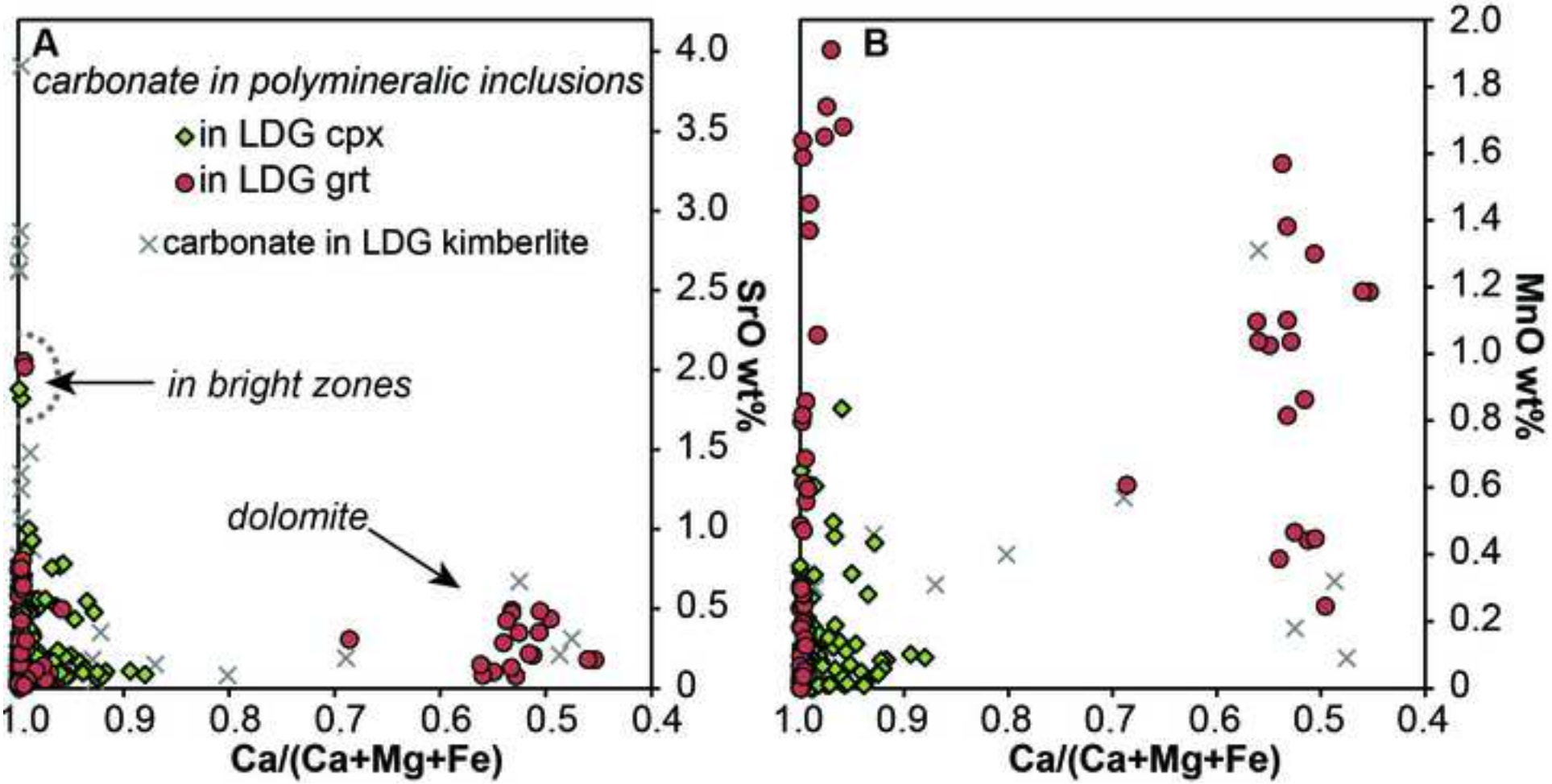

Figure8

Click here to download Figure Fig8.jpg

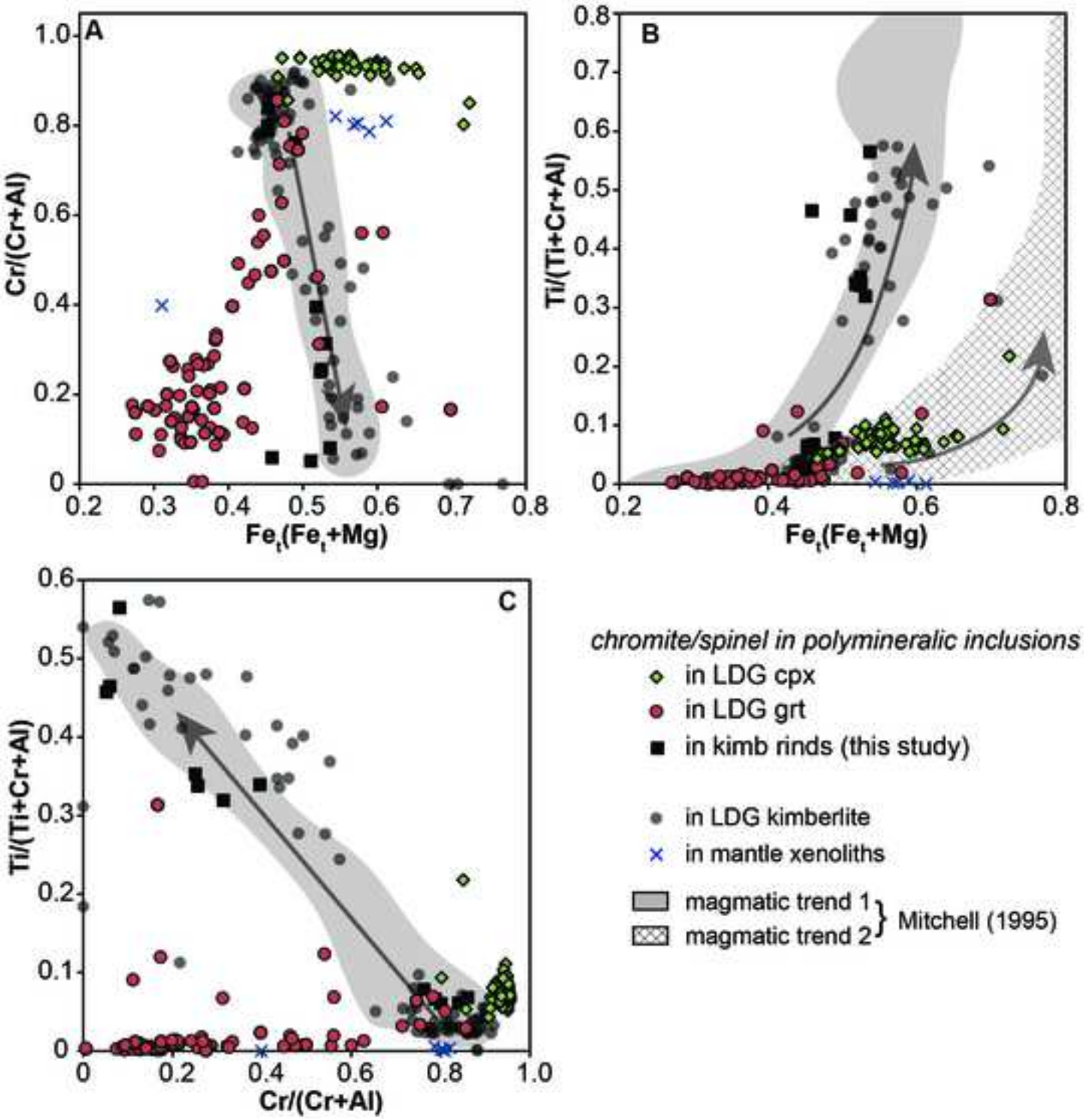

Figure9

Click here to download Figure Fig9.jpg

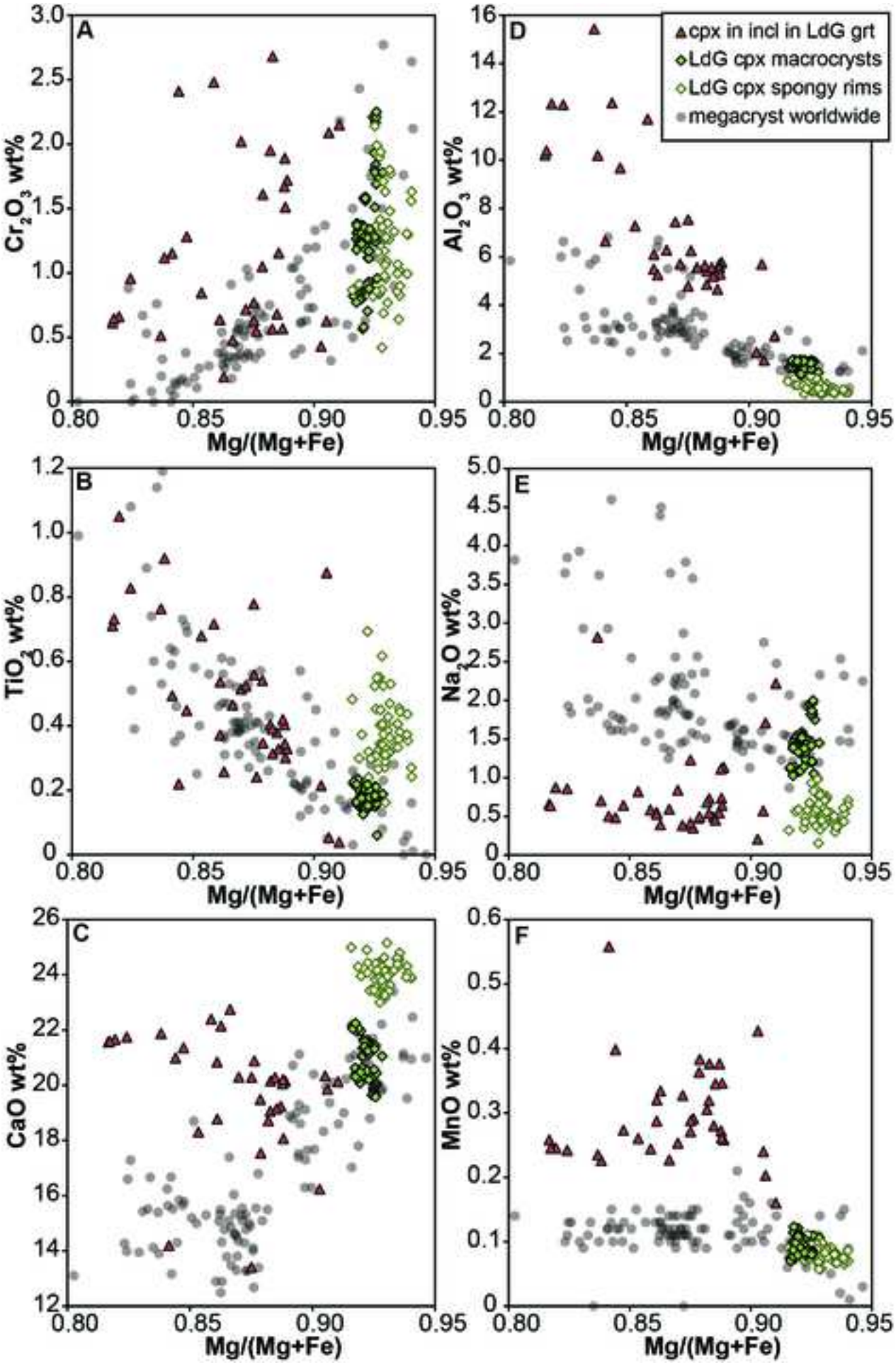

Figure10

Click here to download Figure Fig10.jpg

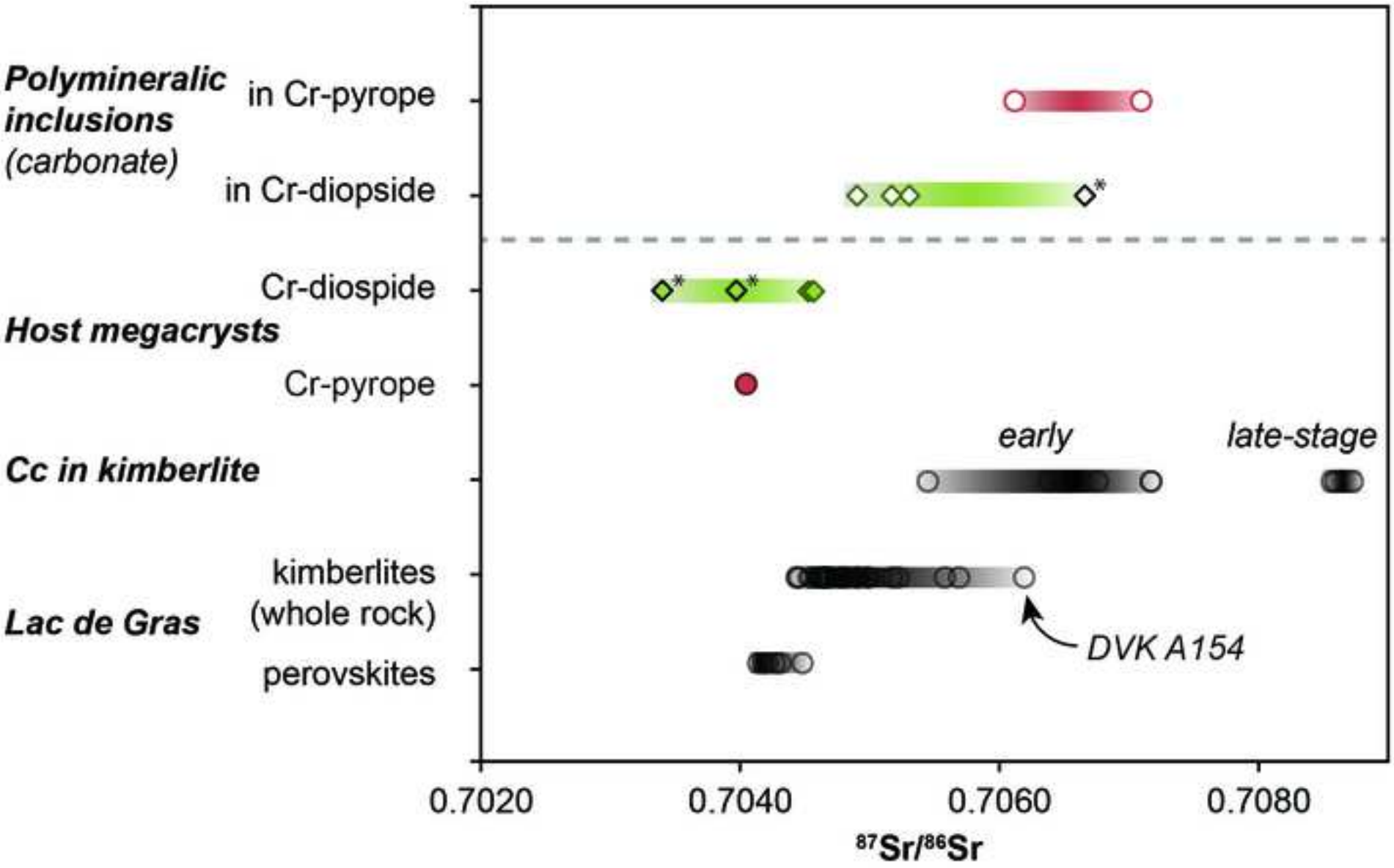

Figure11

Click here to download Figure Fig11.jpg

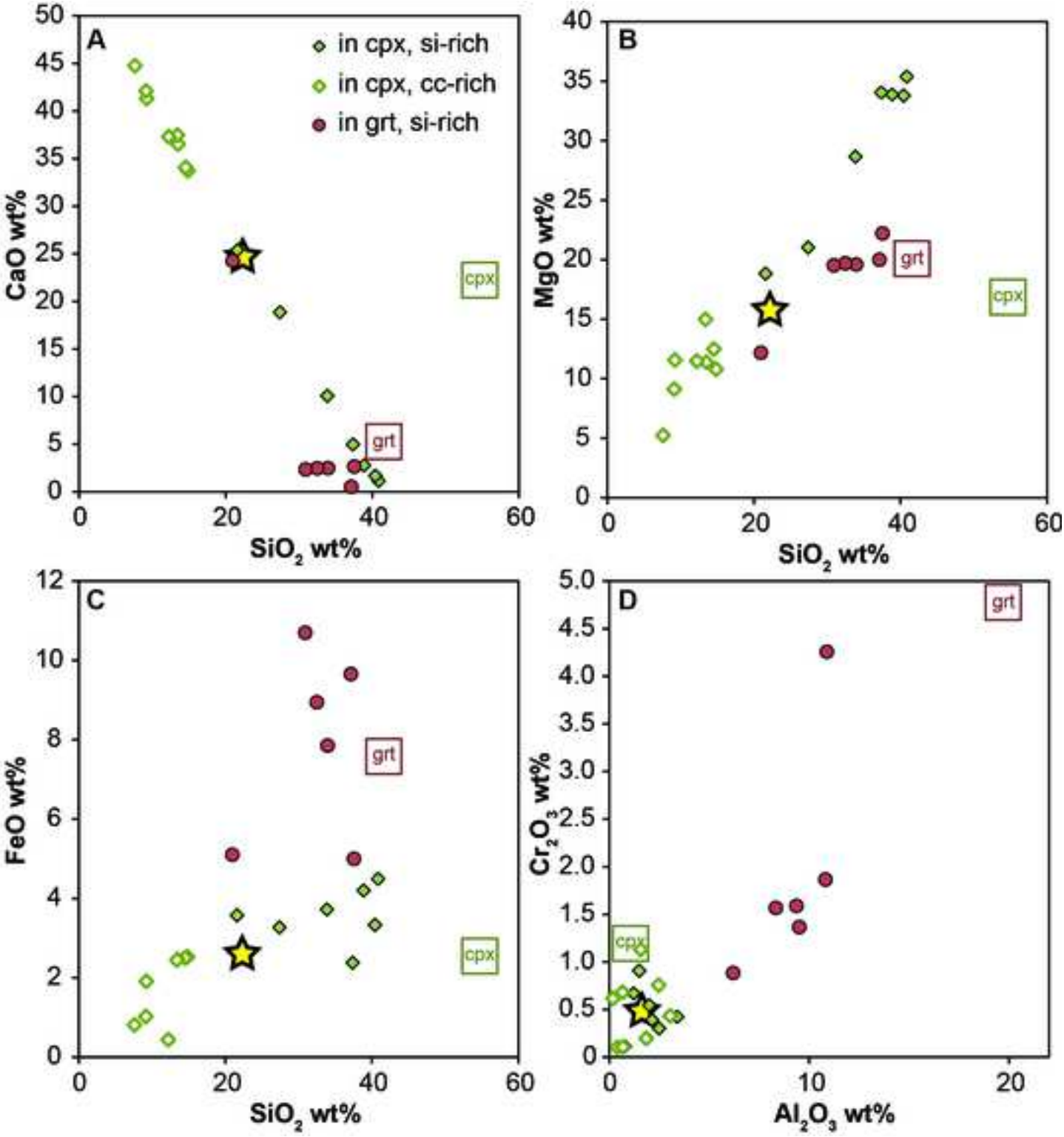

Figure12

Click here to download Figure Fig12.jpg

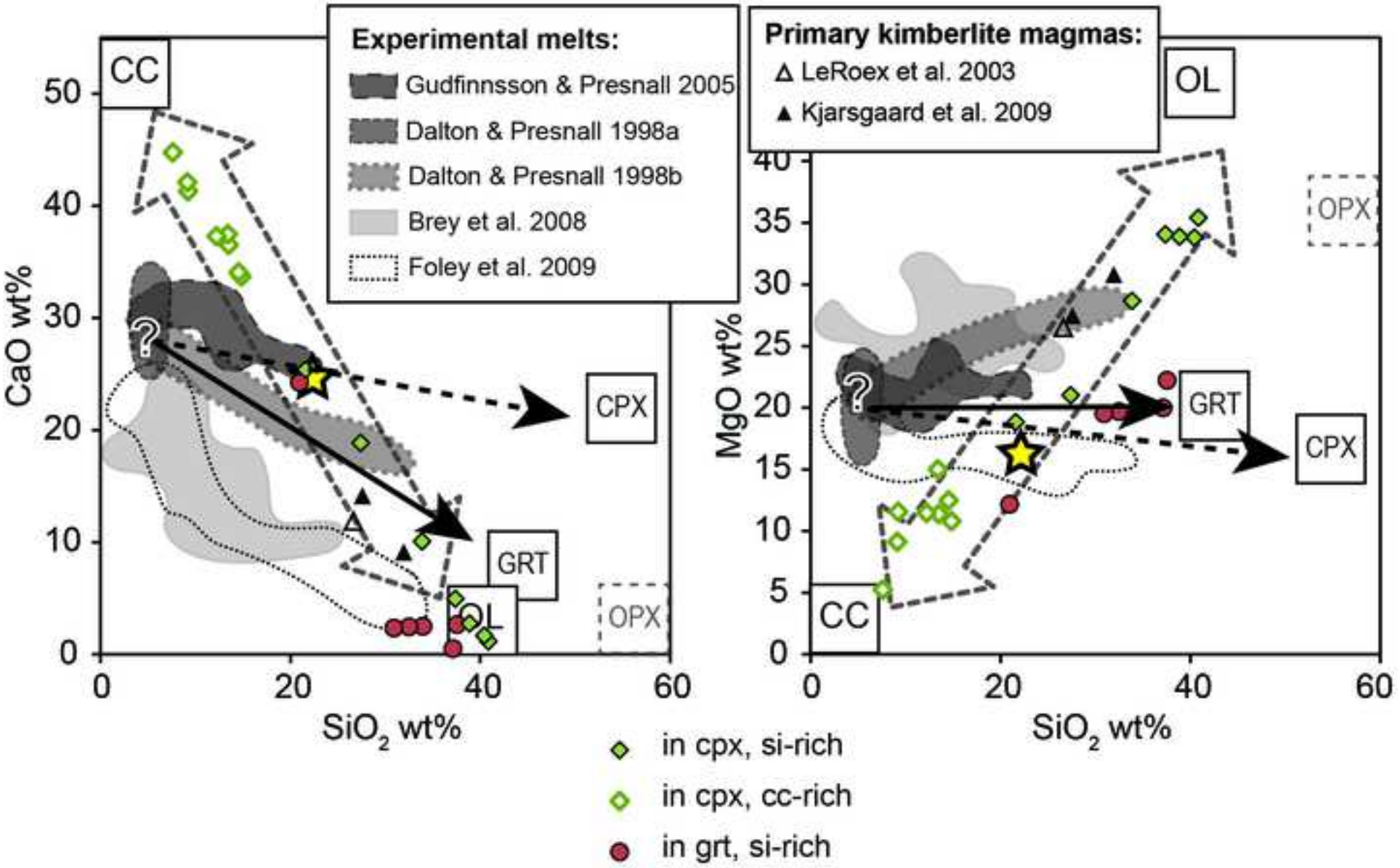

Figure13

Click here to download Figure Fig13.jpg

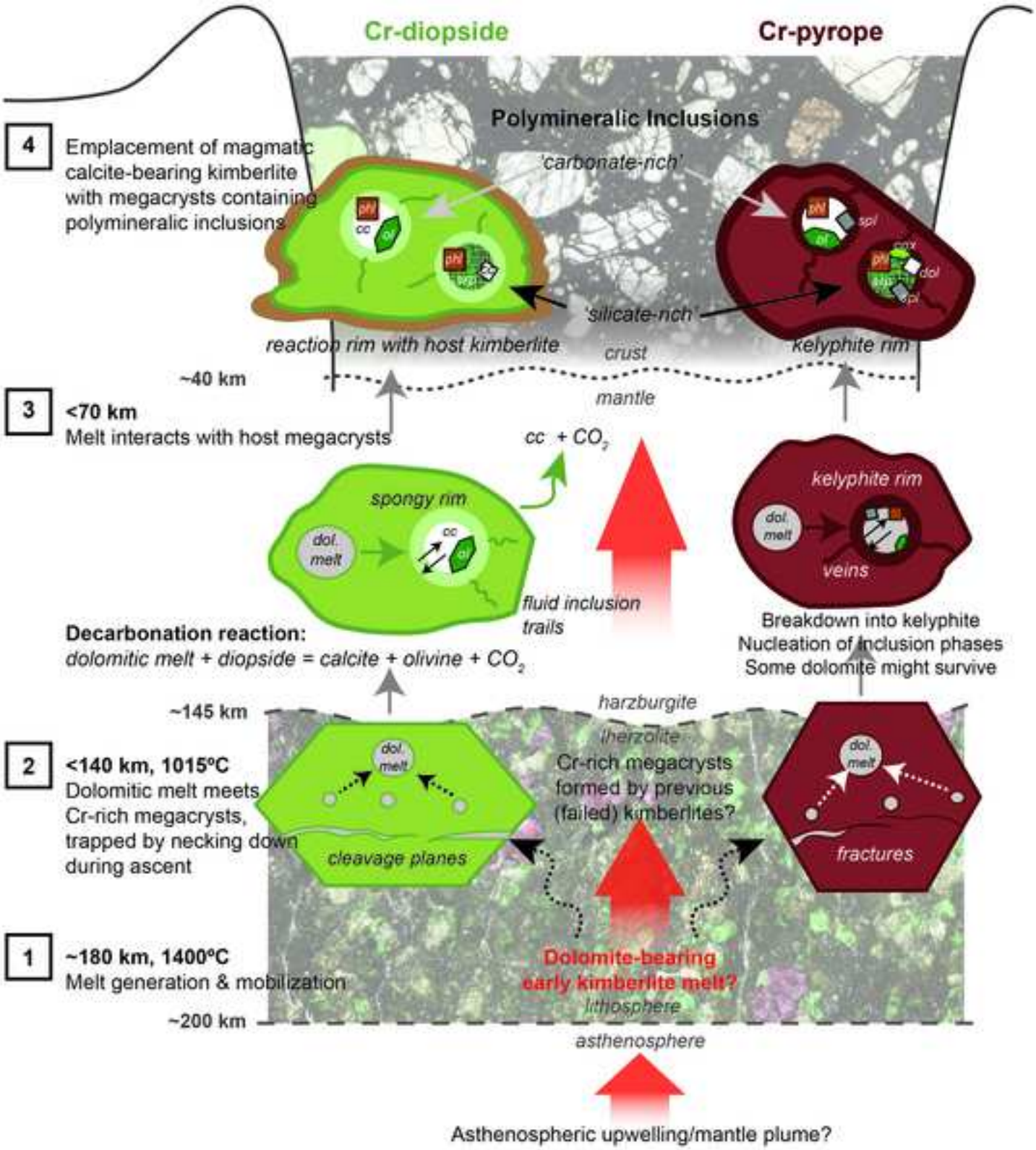

Table 1: P-T results for Cr-diopside megacryst hosts using single-cpx thermobarometry (Nimis and T

Location		Diavik - A154N				
Sample	DVK_CD_04B	DVK_CD_06A	DVK_CD_06B	PL_CD_03 (In01 - 04)	PL_CD_03 (In05)	PL_CD_03 (In06)
T [°C]	1043	1009	1031	1025	965	1040
P [GPa]	5.3	4.6	4.7	4.5	4.2	4.6

Гaylor, 2000)

Ekati - Point lake							
PL_CD_03 (In07 - 08)	PL_CD_03 (In09)	PL_CD_03 (In10)	PL_CD_06 (In01, 04)	PL_CD_06 (In02, 02b)	PL_CD_06 (In03)	PL_CD_07 (In01 - 03)	PL_CD_07 (In04 - 06)
1025	938	1046	1017	1014	997	1043	1011
4.6	4.4	4.5	4.5	4.7	4.5	4.7	4.5

Table 2: Reconstructed bulk compositions of polymineralic inclusions in wt%

Location								
Sample	DVK_CD_01 _In07		DVK_CD_01 _In04		DVK_CD_01 _In02		DVK_CD_01 _In01	
Type	cc-rich		cc-rich		cc-rich		cc-rich	
		1σ		1σ		1σ		1σ
SiO_2	14.8	1.66	14.5	1.63	13.4	1.50	12.2	1.37
TiO_2	0.2	0.02	0.2	0.02	0.1	0.01	0.2	0.02
Al_2O_3	1.6	0.18	3.1	0.34	0.2	0.02	0.7	0.07
Cr_2O_3	1.1	0.13	0.4	0.05	0.6	0.07	0.7	0.08
MnO	0.1	0.01	0.1	0.01	0.5	0.06	1.1	0.12
FeO	2.5	0.28	2.5	0.28	2.4	0.27	0.4	0.05
NiO	-		-		-		-	
MgO	10.8	1.21	12.5	1.40	15.0	1.68	11.5	1.28
CaO	33.7	3.77	34.1	3.81	37.5	4.19	37.3	4.17
BaO	1.3	0.14	-		-		-	
Na_2O	-		0.1	0.01	-		-	
K_2O	0.7	0.08	2.8	0.31	-		0.2	0.03
SrO	0.8	0.09	0.1	0.01	0.1	0.01	0.1	0.01
F	-		0.1	0.01	-		-	
Cl	-		-		-		-	
Total	67.6		70.3		69.9		64.4	
Mg/(Mg+Fe)	0.88		0.90		0.92		0.98	

*overall uncertainty is ~11% and includes uncertainty on modal proportions obtained by QEMSCAN (~

Polymineralic inclusions in clinopyroxene

Diavik - A154N

DVK_CD_01_In08 cc-rich	1σ	DVK_CD_01_In03 cc-rich	1σ	DVK_CD_01_In05 cc-rich	1σ	DVK_CD_6A_In05 si-rich	1σ	DVK_CD_6A_In06 si-rich	1σ
9.2	1.03	9.1	1.02	7.6	0.85	40.9	4.57	40.4	4.52
0.1	0.01	0.1	0.01	0.2	0.02	0.3	0.03	0.4	0.05
0.4	0.05	0.7	0.08	1.9	0.21	2.0	0.22	2.5	0.28
0.1	0.01	0.1	0.01	0.2	0.02	0.5	0.06	0.3	0.03
0.3	0.03	-		-		0.1	0.02	0.1	0.01
1.9	0.21	1.0	0.11	0.8	0.09	4.5	0.50	3.3	0.37
-		-		-		-		-	
11.6	1.29	9.1	1.02	5.2	0.59	35.4	3.96	33.8	3.78
41.3	4.62	42.1	4.71	44.8	5.01	1.2	0.13	1.7	0.19
-		0.1	0.01	0.1	0.01	-		-	
-		-		-		-		0.1	0.01
0.3	0.03	0.5	0.06	1.6	0.18	0.7	0.08	1.3	0.15
0.1	0.01	0.1	0.01	0.1	0.01	-		-	
-		-		0.1	0.01	-		-	
-		-		-		-		-	
65.4		63.0		62.5		85.6		84.0	
0.92		0.94		0.92		0.93		0.95	

5%) and variability of mineral compositions of inclusion phases obtained by EPMA (~10%).

DVK_CD_6A_In03 si-rich		DVK_CD_01_In06 si-rich		DVK_CD_6A_In02 si-rich		DVK_CD_6A_In01 si-rich		DVK_CD_6A_In04 si-rich	
	1σ		1σ		1σ		1σ		1σ
38.9	4.35	37.4	4.18	33.9	3.79	27.4	3.06	21.6	2.41
0.2	0.02	0.2	0.02	0.2	0.03	0.5	0.05	0.2	0.02
1.2	0.14	0.8	0.09	2.2	0.24	3.4	0.38	1.5	0.17
0.7	0.07	0.1	0.01	0.4	0.04	0.4	0.05	0.9	0.10
0.1	0.02	0.1	0.01	0.1	0.01	0.1	0.01	0.1	0.01
4.2	0.47	2.4	0.27	3.7	0.42	3.3	0.37	3.6	0.40
-		-		-		-		-	
33.9	3.79	34.1	3.81	28.7	3.20	21.0	2.35	18.8	2.11
2.8	0.31	5.0	0.56	10.1	1.13	18.9	2.11	25.4	2.84
-		-		-		0.1	0.01	-	
0.1	0.01	-		-		0.1	0.01	-	
0.3	0.04	0.2	0.02	0.8	0.08	2.7	0.30	0.5	0.06
-		-		0.1	0.01	0.1	0.01	0.2	0.02
-		-		-		0.1	0.01	-	
-		-		-		-		-	
82.4		80.1		80.0		77.9		72.9	
0.93		0.96		0.93		0.92		0.90	

Polymineralic inclusions in garnet									
Ekati - Point lake						Ekati - Point lake			
PL_CD_03 _In01 cc-rich		PL_GRT_04 _In14 si-rich		PL_GRT_04 _In7 si-rich		PL_GRT_04 _In04 si-rich		PL_GRT_04 _In05 si-rich	
	1σ		1σ		1σ		1σ		1σ
13.5	1.51	37.6	4.20	37.1	4.15	33.9	3.80	32.5	3.63
0.4	0.04	0.6	0.06	0.4	0.05	0.5	0.05	0.2	0.03
2.5	0.28	8.3	0.93	9.5	1.06	10.8	1.21	9.4	1.05
0.8	0.08	1.6	0.18	1.4	0.15	1.9	0.21	1.6	0.18
0.3	0.04	0.1	0.01	0.1	0.01	0.1	0.01	0.1	0.02
2.5	0.28	5.0	0.56	9.7	1.08	7.9	0.88	8.9	1.00
-		0.1	0.01	0.4	0.04	0.3	0.03	0.4	0.04
11.4	1.27	22.2	2.48	20.0	2.24	19.6	2.19	19.7	2.20
36.5	4.08	2.7	0.30	0.5	0.06	2.5	0.28	2.5	0.28
-		-		-		-		-	
-		0.1	0.01	0.1	0.02	0.2	0.02	0.3	0.04
2.3	0.25	3.2	0.36	5.1	0.57	5.1	0.57	2.9	0.33
0.1	0.02	-		-		-		-	
0.4	0.05	0.1	0.01	0.1	0.01	0.1	0.02	0.1	0.01
-		-		-		-		-	
70.6		81.5		84.4		82.8		78.6	
0.89		0.89		0.79		0.82		0.80	

PL_GRT_04 _In03 si-rich		PL_GRT_04 _In13 si-rich	
	1σ		1σ
30.9	3.46	20.9	2.34
0.3	0.04	0.6	0.06
10.9	1.22	6.2	0.69
4.3	0.48	0.9	0.10
0.1	0.02	0.1	0.01
10.7	1.20	5.1	0.57
0.3	0.03	0.2	0.02
19.5	2.18	12.2	1.36
2.4	0.26	24.3	2.71
-		-	
0.4	0.04	0.1	0.01
1.5	0.17	3.1	0.35
-		-	
-		0.3	0.03
-		-	
81.3		73.9	
0.76		0.81	